TRENDS IN SCIENCES 2026; 23(2): 11699
https://doi.org/10.48048/tis.2026.11699
REVIEW ARTICLE

Research Progress on the Separation and Recycling of Cathode Materials for Lithium Iron Phosphate Waste Batteries

Aichun Dou[1], Qingshan Du[1], Zhixiong Yan[2], Yunjian Liu[1], Luping Liu[2,*], Yuqian Fan[1] and Zejian Bai[1]

[1]*School of Material Science and Engineering, Jiangsu University, Zhenjiang 212013, China*
[2]*Zhejiang New Era Zhongneng Technology Co., Ltd, Shaoxing, China*

(*Corresponding author's e-mail: sarsasds@163.com)

Received: 26 August 2025, Revised: 28 October 2025, Accepted: 5 November 2025, Published: 30 November 2025

Abstract

The rise of electric vehicles has led to the increasing use of lithium iron phosphate batteries, and a large number of lithium-ion batteries are facing urgent need for recycling due to close to the end of their service life. This paper reviews the current status of recycling used lithium iron phosphate batteries and introduces the main recycling processes, which are pyrometallurgical recycling, hydrometallurgical recycling, and direct recycling. This paper focuses on the separation and recycling technologies of current cathode materials. This review further explores the latest methods and research advances in the separation and recycling of cathode materials, providing a critical analysis of the core challenges and future development prospects of existing process technologies. Through a comparative assessment of various recycling methods, this review proposes an optimized strategy with potential for industrial-scale application. This strategy shifts away from the conventional "leaching-impurity removal-separation" paradigm, which relies on complex separation steps, and instead emphasizes the most advanced and promising green recycling strategies for spent lithium iron phosphate (LFP) batteries: Namely, "selective leaching" and "direct regeneration."

Keywords: Lithium iron phosphate batteries, Spent lithium iron phosphate, Recycle, Pre-process, Hydrometallurgy, Pyrometallurgy, Direct regeneration

Introduction

Lithium-ion batteries (LIBs) have the advantages of high energy density, excellent cycling performance, and high operating voltage, which have been widely used in fields such as energy storage, automotive systems, consumer electronics, electric vehicles and agricultural machinery [1-4]. In terms of energy storage, lithium-ion batteries and new energy storage devices such as supercapacitors (SC) are receiving increasing attention [5,6]. Currently, LIBs can be categorized into lithium cobalt oxide (LCO), lithium manganese oxide (LMO), lithium iron phosphate (LFP), and $LiNi_xCo_yMn_{1-x-y}O_2$ (NCM) based on cathode material composition [7]. The cathode material directly affects the overall performance of the power battery and plays a crucial role in its operation. Compared with other lithium-ion battery cathode materials, the olivine-shaped structure of LFP exhibits a lower electrochemical potential [8]. The phosphate (PO_4^{3-}) tetrahedra in the LFP structure form stable P-O covalent bonds that contribute to enhanced thermal stability. Therefore, LFP has been recognized as an intrinsically safe cathode material [9,10]. Industry projections indicate that electric vehicle adoption of this battery technology is expected to peak by 2030. Global LFP battery capacity is projected to reach 463 GWh, representing 25 times that of 2019 levels [11]. The limited-service life of LFP batteries typically ranges from 5 - 10 years [12]. With the growing deployment of LFP batteries, this will lead to significant accumulation of spent lithium iron phosphate (SLFP) batteries at the end of the battery life [13]. SLFP batteries contain

hazardous components including electrolytes and heavy metal compounds. Improper management may result in severe environmental risks through soil degradation and water system contamination [14-16]. Concurrently, these SLFP batteries retain substantial concentrations of valuable metallic elements [17]. Lithium emerges as the most economically significant constituent, constituting 1% - 2% of battery mass. Effective lithium recovery therefore presents dual benefits: reducing manufacturing costs while mitigating critical metal resource scarcity.

However, fewer than 5% of used lithium-ion batteries undergo recycling processes due to high economic costs and technical complexities [18]. Resolving the shortcomings of current recycling methods constitutes a priority requirement for efficient recovery of lithium resources.

SLFP batteries feature a multilayered structure containing metallic casing, electrode active materials, polymer separator, and liquid electrolyte [19]. They contain valuable elements such as lithium (Li), iron (Fe), phosphorus (P), copper (Cu), aluminum (Al) and graphite that are worth recycling, as well as hazardous substances containing fluorine electrolytes, organic solvents, and polymer binders that are highly risky and harmful to the environment [20]. This makes the efficient recycling of SLFP batteries a key aspect of resource recycling and environmental protectio [21]. Recycling of spent lithium batteries starts with pretreatment. SLFP batteries undergo deep-discharging to eliminate residual energy, followed by sequential mechanical processing steps: Discharging, disassembling, crushing, and sieving. These preparatory operations enable effective liberation of LFP cathode material from aluminum current collectors, polymer separators, and ancillary components.

Currently, the traditional methods of recovering SLFP materials are mainly pyrometallurgy, hydrometallurgy and direct regeneration. Pyrometallurgy utilizes high-temperature smelting to convert lithium species in used batteries into lithium salts to achieve recovery [22]. The simple and easy process characteristics make pyrometallurgy widely used in the first few years. Its requirements for high temperature and vacuum environment are strict, often accompanied by a large amount of energy consumption and the emission of fluoride and other toxic gases [23-25]. The smelting products are mostly in the form of alloying, the output rate is low, and the subsequent separation and recycling have significant difficulties. These inherent technical constraints significantly undermine pyrometallurgy's economic viability and industrial applicability [11,26].

Hydrometallurgy mainly realizes metal recovery by dissolving electrode materials in acidic solution, which has the advantages of low energy consumption, high metal recovery rate, and high product purity compared with the thermal process [27-30]. It is mainly divided into 2 categories: Inorganic acid leaching and organic acid leaching. Conventional inorganic approaches employ mineral acids for rapid extraction, such as HCl, H_2SO_4, HNO_3. However, the use of excess strong acid needs to be neutralized by alkali, and the processes produce a large amount of wastewater and harmful gases to increase the cost of environmental protection treatment [31,32]. In contrast, organic acids like HCOOH, CH_3COOH and $C_6H_8O_7$ have been explored for leaching $LiFePO_4$ materials. Organic acid leaching can avoid the use of strong acid and alkali, and can greatly reduce the emission of waste gas and water [33]. However, organic acid leaching usually requires an oxidizing agent such as hydrogen peroxide and a long reaction time [34-36]. Nevertheless, with the growing complexity of battery material sources, recycling technologies must evolve from processing single components to managing mixed waste streams. Moreover, conventional acid leaching processes are plagued by considerable environmental and economic drawbacks. Consequently, future research should prioritize the development of green alternatives that feature low energy consumption, minimal pollution, and reduced corrosivity [37].

During the repeated charge and discharge cycles of LFP batteries, part of the Li^+ cannot completely return to the cathode body, resulting in Li^+ vacancies in the cathode material [38]. This is the main reason for the capacity degradation of LFP batteries. Subsequent multiple battery charging and discharging will continue to increase the loss of lithium in the cathode, and the continuous accumulation of a large number of lattice vacancies lead to irreversible loss of active lithium. This method has the advantages of simple production process, lower production cost, and less waste emission compared to the previous two processes. However, the chemical properties and purity of the products obtained

from the regenerated materials vary due to impurity residues [39-41]. The current methods for direct regeneration of LFP include high temperature solid-phase regeneration, the water heat method, and the electrochemical regeneration method [42-44].

This review provides a systematic outline of the pretreatment framework and lithium recovery strategies for spent lithium iron phosphate (SLFP) batteries. It examines the fundamental mechanisms, technological progress, and persistent challenges associated with three mainstream cathode recycling methods. A comparison of the economic and environmental profiles of different processes clarifies their respective technical limitations and suitable application scenarios. The discussion then focuses on the latest advances in the separation and recycling of cathode materials, offering a critical analysis of the core issues and future directions for existing technologies. Based on a comparative assessment of various recycling methods, an optimized viewpoint with high potential for industrial-scale application is proposed. This viewpoint represents a paradigm shift, moving away from the traditional "leaching-impurity removal-separation" model reliant on complex steps. Instead, it champions the most advanced and promising green strategies for SLFP battery recycling: "selective leaching" and "direct recycling."

Materials and methods

In April 2025, a comprehensive literature search was conducted using the Web of Science database (all databases). Search and organize key information on lithium iron phosphate batteries, recycling, pretreatment, pyrometallurgy, hydrometallurgy, and direct regeneration recycling (in any topic, title or text). Based on the theme of recycling waste lithium iron phosphate batteries, this study screened and analyzed articles published in the past 5 years or classic literature in this recycling field. Ultimately, this review identified 10 academic papers related to pretreatment, 5 academic papers on SLFP pyrometallurgical recycling, 10 academic papers on SLFP hydrometallurgical recycling, and 6 academic papers related to direct recycling. A detailed and in-depth analysis of the aforementioned articles was conducted, providing a comprehensive discussion of the methods, principles, and process conditions for recycling used lithium iron phosphate batteries mentioned in the articles. From the available studies, information regarding 1) pretreatment of used lithium iron phosphate batteries; 2) pyrometallurgical recycling of used lithium iron phosphate; 3) hydrometallurgical recycling of used lithium iron phosphate and 4) direct recycling of used lithium iron phosphate.

Results and discussion

Pre-processing of spent phosphate batteries

Retired lithium iron phosphate batteries are usually disassembled directly from cars or other places, and these batteries usually carry about 70% residual power. A large amount of power residue will make the disassembly process easy to trigger thermal runaway phenomenon, which may lead to heat accumulation, inducing the risk of combustion and explosion [45]. Therefore, used lithium iron phosphate batteries need to be fully discharged before pretreatment [46]. At present, the discharge of used lithium batteries is divided into physical and chemical two. Physical discharge can achieve rapid discharge by external load or forced short circuit without consuming chemical reagents. However, the consumption of a large amount of power will cause the battery temperature to rise sharply, there is a potential risk of thermal runaway [47]. Chemical discharge consumes the remaining power with the help of electrolyte. However, the addition of extra chemicals may also lead to oxidative corrosion of Fe and Al, which have high reduction potentials in the cathode material [48]. After discharge, the battery is disassembled according to the physicochemical properties of the elements in the lithium-ion battery [49]. Such as disassembling into independent components such as positive pole piece, negative pole piece, shell, plastic [50]. Or directly mechanically crushed into black powder consisting of cathode, anode, aluminum (Al) foil, copper (Cu) foil with graphite [51]. Differences in pretreatment processes directly affect the choice of subsequent recovery routes.

Discharge treatment of SLFP batteries

Conductive powder particle discharge is a commonly used physical discharge method. Conductive dielectrics, such as copper, graphite, and iron powders, are used for the physical discharge of lithium-ion batteries [52]. A short circuit loop is formed by bridging

the electrodes through a resistor, which is able to dissipate the residual electrical energy quickly. This technique has significant engineering advantages in small-capacity battery disposal due to its high-efficiency discharge characteristics.

Nan *et al*. [53] conducted short-circuit discharge on used LIB batteries in a stainless-steel container containing water and iron powder. The residual charge was completely discharged within about 30 minutes with mechanical agitation. Zhan *et al.* [54] connected experimental LIB batteries to a load (halogen bulb) and discharged them at a potential of 1.0 - 2.0 V. Chemical discharge through conductive solutions formulated with salts, acids or bases is the main method for electrical energy consumption in used LIB batteries. While saturated sodium chloride solutions are commonly used for complete discharge, they can severely corrode the battery casing, making it unsuitable for reuse [55]. Xiao *et al*. [56] controlled oxygen levels during discharging in $MnSO_4$ solution to reduce iron corrosion and prevent organic leakage, effectively inhibiting galvanic coupling reactions. During discharge in $MnSO_4$ solution, a protective layer forms at the anode, effectively preventing oxygen corrosion. Additionally, this study investigated the discharge performance of different salt solutions. As shown in **Figure 1(A)**, the battery discharges rapidly in NaCl solutions of varying concentrations, experiencing severe electrochemical corrosion and solution discoloration to yellow due to Cl^-. The discharge behavior of batteries in partial sulfate, nitrate, and chloride solutions is shown in **Figure 1(B)**. NaCl and KCl solutions achieve rapid discharge, but the battery structure is severely damaged after discharge. As discharge time increases, the discharge efficiency of $MnSO_4$ solution remains relatively stable. The changes in the discharge process of the battery in salt solutions and the XRD spectra of the flocculent precipitates generated during the discharge process are shown in **Figure 1(C)**. During discharge in NaCl, KCl, $NaNO_3$, and $MgSO_4$ solutions, the iron casing undergoes significant galvanic corrosion accompanied by flocculent precipitates of varying colors. However, no flocculent deposits were observed in the $MnSO_4$ solution after discharge, indicating suppressed corrosion, thereby reducing organic leakage. This suggests that the O_2 control mechanism in the $MnSO_4$ solution can effectively reduce battery galvanic corrosion and organic leakage. The mechanism of battery discharge in the $MnSO_4$ solution is shown in **Figure 1(D)**. Garg *et al*. [57] proposed utilizing the Fe(II)-Fe(III) redox couple in electrolytes for deep LIB discharge. Iron/ferricyanide redox pair facilitated oxidation and reduction reactions at battery poles, consuming electrons to achieve battery discharge.

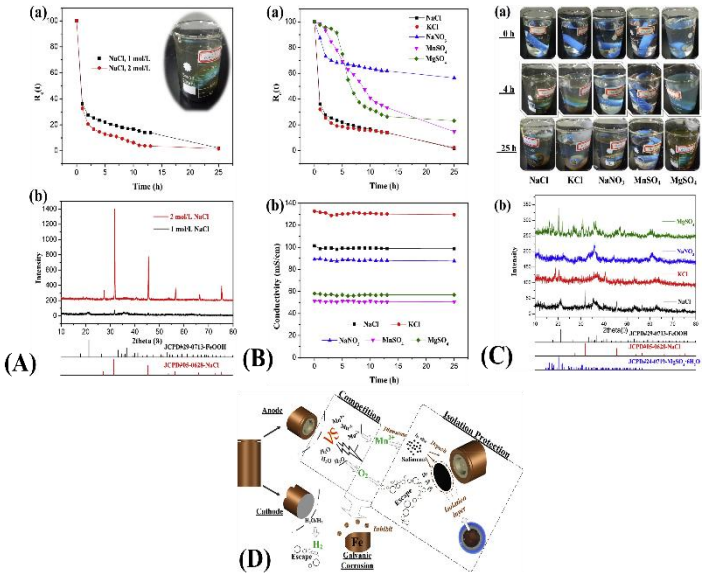

Figure 1 (A) (a) Discharge curves of LIBs in different concentrations of NaCl solution and (b) XRD patterns of the filtered flocks [56]. (B) Change curves of (a) battery voltage and (b) conductivity in different saline solutions with time (the molarity: 1 mol/L) [56]. (C) (a) The discharge processes of batteries in saline solutions (molarity: 1 mol/L); (b) XRD patterns of filtered flocks [56]. (D) Proposed reaction mechanism for the batteries discharge in $MnSO_4$ solution [56].

Dismantle of SLFP batteries

The disassembly and separation of used LIB batteries are achieved by physical means to enable pre-enrichment of key components such as Li, Co, and Cu, which are then combined with leaching and recovery technologies to further purify and recycle these valuable materials [52]. Battery dismantling is mainly divided into 2 categories: Manual dismantling and mechanical dismantling. Manual dismantling primarily uses tools such as pliers and saws to strip components layer by layer, a process that is inefficient and time-consuming. This method is only applicable for processing small quantities of used batteries, such as in laboratory-scale studies [58]. Mechanical disassembly using crushers or hammer mills can achieve large-scale industrial recycling of waste LIB batteries. However, the disassembled materials are prone to mixing, and tiny components cannot be completely separated, leading to reduced electrode material recovery rates [59]. Both methods carry risks of toxic electrolyte leakage. Electrolyte treatment involves two approaches: high-temperature roasting and low-temperature freezing. High-temperature roasting causes the electrolyte to evaporate at elevated temperatures but generates toxic gases.

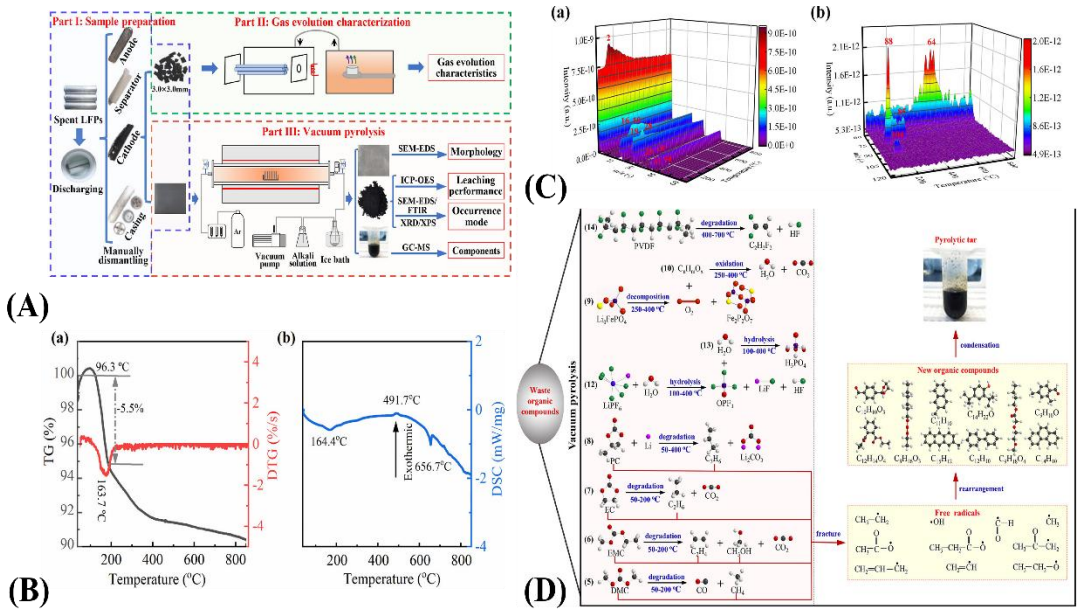

Figure 2 (A) Flowsheet of experimental process for spent cathode plates recovery [60]. (B) (a) TG-DTG curves and (b) DSC curve of spent cathode plates at different temperatures [60]. (C) TG-DSC-EI-MS analysis of gases evolved from the spent cathode plates at different temperatures. (a) Three-dimensional (3D) mass spectrum graph of evolved gases measured at low channels. (b) 3D mass spectrum graph of evolved gases measured at high channels [60]. (D) Illustration of thermal degradation mechanism of electrolyte solvents [60].

Jie *et al.* [60] investigated the desorption behavior of gaseous products and the recovery performance of cathode materials during SLFP vacuum pyrolysis. The process flow of SLFP vacuum pyrolysis recovery is shown in **Figure 2(A)**. Thermal gravimetric analysis (TGA) was performed on generated gases, with results shown in **Figure 2(B)**. Between 26 and 184 °C, electrolyte evaporation and hydrolysis caused rapid 5.5 wt% weight loss. As temperature increases to 400 - 650 °C, weight loss slows and changes in this range are related to polyvinylidene fluoride (PVDF) decomposition. At 656.7 °C, an endothermic peak occurs due to aluminum foil melting, and a further temperature increase leads to $LiFePO_4$ decomposition. Therefore, pyrolysis temperature should be controlled between 500 and 600 °C. Gaseous products were characterized using TG-DSC-EI-MS (**Figure 2(C)**). Based on ion current intensity curves, the primary gaseous products are identified as inorganic gases, alkane gases, and fluorinated gases. The pyrolysis process is divided into three distinct phases based on products (**Figure 2(D)**): The first phase (50 - 400 °C)

produces mainly inorganic/alkane gases; the second phase involves $LiPF_6$ hydrolysis; the third phase is PVDF degradation at 400 - 700 °C with $C_2H_2F_2$ as the main product. Grandjean *et al.* [61] proposed a method of dismantling waste lithium batteries using cryogenic freezing. Experiments showed that even under extreme conditions, the dismantling process releases no energy, and thermal runaway is completely eliminated. Furthermore, after five repeated cryogenic cycles, rapid freezing does not affect the electrochemical performance of the batteries. Cryogenic freezing uses liquid nitrogen to solidify the electrolyte at ultra-low temperatures, a process requiring substantial liquid nitrogen consumption that increases recycling costs.

Recovery of SLFP powders

There are three main methods for separating aluminum foils and active substances. The first method utilizes organic solvents based on the principle of similar-phase solubility. Certain high-polarity organic solvents are employed to dissolve the PVDF binder. Commonly used organic solvents include N-methylpyrrolidone (NMP), N,N-dimethylformamide (DMF), and N,N-dimethylacetamide (DMAC). He *et al.* [62] experimentally evaluated the separation performance of different solvents and the effect of ultrasonic-assisted cleaning. During the separation of waste lithium-ion batteries, it is inevitably difficult due to the strong bonding force between the cathode material and the aluminum foil, complicating separation. This study employs ultrasound to assist in separating the aluminum foil from the cathode material. The effects of solvent properties, temperature, ultrasound power, and ultrasound duration on separation efficiency were investigated, utilizing polyvinylidene fluoride (PVDF) dissolution and cavitation effects under ultrasound. Experimental data revealed that under optimized conditions (70 °C process temperature, 240 W ultrasonic power, 90 min ultrasonic duration), the N-methyl-2-pyrrolidone (NMP) cleaning solution enabled 99% separation efficiency between the cathode material and aluminum foil. The aluminum foil showed no significant agglomeration after ultrasonic peeling, facilitating subsequent leaching and recycling processes for waste batteries. Additionally, NMP and other organic solvents demonstrated significant potential for separating aluminum foil from cathode materials, however, their high cost and volatility pose challenges to worker safety and environmental protection in industrial applications.

Table 1 Recovery of Li by different roasting methods in pyrometallurgy.

Pre-processing	Methods	References
Discharge	Short-circuit discharge of water and iron powder	[53]
	Halogen bulb discharge	[54]
	Discharge of NaCl solution	[55]
	Discharge of $MnSO_4$ solution	[56]
Dismantle	Manual dismantling	[58]
	Mechanical dismantling	[59]
	Vacuum pyrolysis	[60]
	Cryogenic freezing	[61]
Recovery of SLFP powders	High-polarity organic solvents	[62]
	Acid-base selective dissolution	[63]

The second separation method involves calcining the cathode sheet in a muffle furnace at high temperatures to decompose the binder. The melting point difference between PVDF (approximately 400 °C) and aluminum (approximately 650 °C) enables their differentiation. The third method employs acid-base selective dissolution to achieve material separation. Based on aluminum foil's solubility in alkaline solutions, Fu *et al.* cut disassembled cathode materials into 1×1 cm^2 pieces and dissolved aluminum foil surfaces in dilute alkaline solutions to separate LFP from aluminum foil [63]. In this study, the dissolution of aluminum foil surfaces was achieved using a dilute alkaline solution. Separation of aluminum foil from cathode active material was realized under low-energy, low-cost conditions with minimal aluminum foil loss. Key factors influencing separation efficiency were investigated: alkaline solution concentration, liquid-solid ratio, and stirring time. Optimal conditions were determined as 0.075 mol/L alkaline solution, 20 mL/g liquid-solid ratio, and 40-min stirring time. Although simple to operate, this process generates waste salt solution requiring additional treatment. Furthermore, separated products often contain residual impurities, increasing difficulty in subsequent purification. Various pretreatment methods for waste lithium batteries are shown in **Table 1**.

Pyrometallurgical recovery

Pyrometallurgical recovery of SLFP utilizes high-temperature smelting to convert extractable lithium elements into recoverable lithium salts. This method reduces reliance on strong acid and alkali reagents while maintaining a simple process flow with high adaptability, facilitating large-scale industrial implementation. Pyrometallurgical recovery mainly involves direct roasting and molten salt-assisted roasting.

Direct roasting

Direct roasting primarily recovers carbon or aluminum as reducing agents through metal alloy formation in high-temperature environments for cathode material reduction. However, $LiFePO_4$'s stable olivine structure prevents direct carbon reduction. Zhang *et al.* [64] proposed a novel carbothermal reduction method using Na_2CO_3 as an activator to decompose LFP. With Na_2CO_3 assistance, LFP's chemical bonds are disrupted, enabling carbothermal reduction to produce Fe, $NaLi_2PO_4$, and $LiNa_5(PO_4)_2$, which are subsequently separated via magnetic techniques. The optimal process parameters with LFP/Na_2CO_3 molar ratio of 1:1, LFP/graphite ratio of 1:2, and 900 °C roasting for 4 h are shown in **Figure 3(A)**. The immersion rate of Li is more than 90%. **Figure 3(B)** shows that there is a two-stage carbothermal reduction process (1) molten Na_2CO_3 disrupting Li-O/Fe-O bonds by encapsulating LFP to form intermediate FeO, and (2) graphite-assisted FeO decomposition where Fe captures oxygen, collapsing FeO_6 octahedra to release CO_2. The whole reaction process is shown in Eqs. (1) - (3). Residual PO_4^{3-} combines with Na^+/Li^+ to form stable $Li_xNa_yPO_4$ complexes. The Na_2CO_3-assisted roasting method demonstrates innative carbothermal reduction of SLFP through a simplified, efficient recovery process with industrial feasibility.

Formation of intermediate FeO

$$3LiFePO_4 + 3Na_2CO_3 = 3FeO + NaLi_2P0_4 + Li\ Na_5(PO_4)_2 + 3CO_2(g) \quad (1)$$

Reduction of intermediate FeO by carbon

$$C + 2FeO = 2Fe + CO_2(g) \quad (2)$$

The overall reaction is

$$3LiFePO_4 + 3Na_2CO_3 + 1.5C = 3Fe + NaLi_2PO_4 + LiNa_5(PO_4)_2 + 4.5CO_2(g) \quad (3)$$

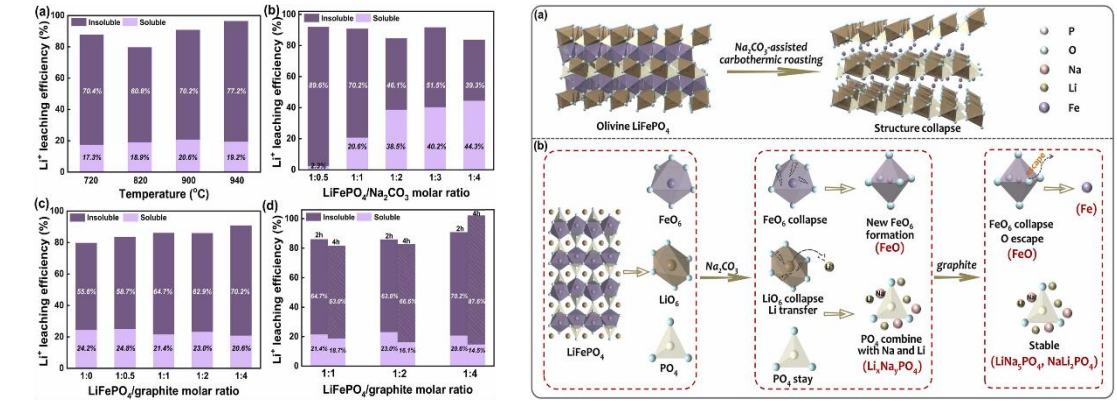

Figure 3 (A) Li^+ leaching efficiencies for Na_2CO_3-assisted carbothermic roasting under (a) different roasting temperatures (LFP/ Na_2CO_3 molar ratio = 1:1, LFP/graphite molar ratio = 1:4, 2 h), (b) different LFP/ Na_2CO_3 molar ratios (LFP/graphite molar ratio = 1:4, 900 ℃, 2 h), (c) different LFP/graphite molar ratios (LFP/ Na_2CO_3 molar ratio = 1:2, 900 ℃, 2 h), and (d) different roasting times (LFP/ Na_2CO_3 molar ratio = 1:2, 900 ℃) [64]. (B) Schematic illustration of the conversion mechanism for the Na_2CO_3-assisted carbothermic roasting of LFP [64].

Molten salt-assisted roasting

The use of sulfate, bisulfate, and sodium salts in acid-free environments enables effective SLFP recovery and separation while avoiding acidic wastewater treatment and environmental concerns. Qu *et al.* [65] developed a lithium extraction and $FePO_4$ recovery method from crystalline $LiFePO_4$ using ammonium sulfate $(NH_4)_2SO_4$-assisted rapid roasting, as shown in **Figure 4(A)**. Optimal parameters included 300 °C roasting temperature, the ratio of C-LFP to $(NH_4)_2SO_4$ is 1:0.8, 10-minute duration, and air atmosphere, achieving 97.80% lithium extraction with less than 2% iron dissolution. Eqs. (4) - (11) show the reactions that occur in roasting under different atmospheres, the reaction principle is shown in **Figure 4(B)**. The TG-DSC images under different atmospheres are shown in **Figure 4(C)**. The reactions of assisted roasting of $(NH_4)_2SO_4$ under air atmosphere involve, in turn, the vaporization of $(NH_4)_2SO_4$, and the synergistic interaction of $(NH_4)_2SO_4$ with O_2. The thermal instability of $(NH_4)_2SO_4$ and its intermediate products necessitates lower temperatures and shorter reaction times to maintain roasting efficiency while reducing costs. Sodium bisulfate-assisted process utilizes molten sulfuric acid from $NaHSO_4$ decomposition as secondary sulfide [66]. Molten Na_2SO_4 promotes H^+-Li^+ exchange within the Fe-P-O structure. Under optimized conditions (mass ratio of $NaHSO_4 \cdot H_2O$ to LFP is 1.5:1, 600 °C/1 h roasting, 30 °C/1 h leaching), 98.12% Li leaching efficiency was achieved with < 1% Fe, Al, and P dissolution. Recovered $LiFePO_4$ exhibited 140.99 mAh/g discharge capacity at 1 C over 200 cycles, maintaining 96.57% capacity retention.

The thermal decomposition of $(NH_4)_2SO_4$

$$NH_4)2SO_4 = NH_4HSO_4 + NH_3(g) \quad (4)$$

$$NH_4HSO_4 = 0.5(NH_4)_2S_2O_7 + 0.5H_2O(g) \quad (5)$$

$$0.5(NH_4)_2S_2O_7 = 1/3NH_3(g) + 1/3N_2(g) + SO_2 + 0.5H_2O(g) \quad (6)$$

Over all reaction

$$(NH_4)_2SO_4 = 4/3NH_3 + 1/3NH_3(g) + 1/3N_2(g) + SO_2 + 2H_2O(g) \quad (7)$$

Sulfation roasting in air

$$2LiFePO_4 + 0.5O_2 + (NH_4)_2SO_4 = Li_2SO_4 + 2FePO_4 + 2NH_3(g) + H_2O(g) \quad (8)$$

$$2LiFePO_4 + O_2(g) + SO_2 = Li_2SO_4 + 2FePO_4 \quad (9)$$

Sulfation roasting in Ar or vacuum

$$LiFePO_4 + 0.5(NH_4)_2S_2O_7 = 0.5Li_2SO_4 + FePO_4$$

$$+ 0.5SO_2 + NH_3 + 0.5H_2O \quad (10)$$

$$LiFePO_4 + (NH_4)_2SO_4 = 0.5Li_2SO_4 + FePO_4 + 0.5SO_2 + 2NH_3 + H_2O \quad (11)$$

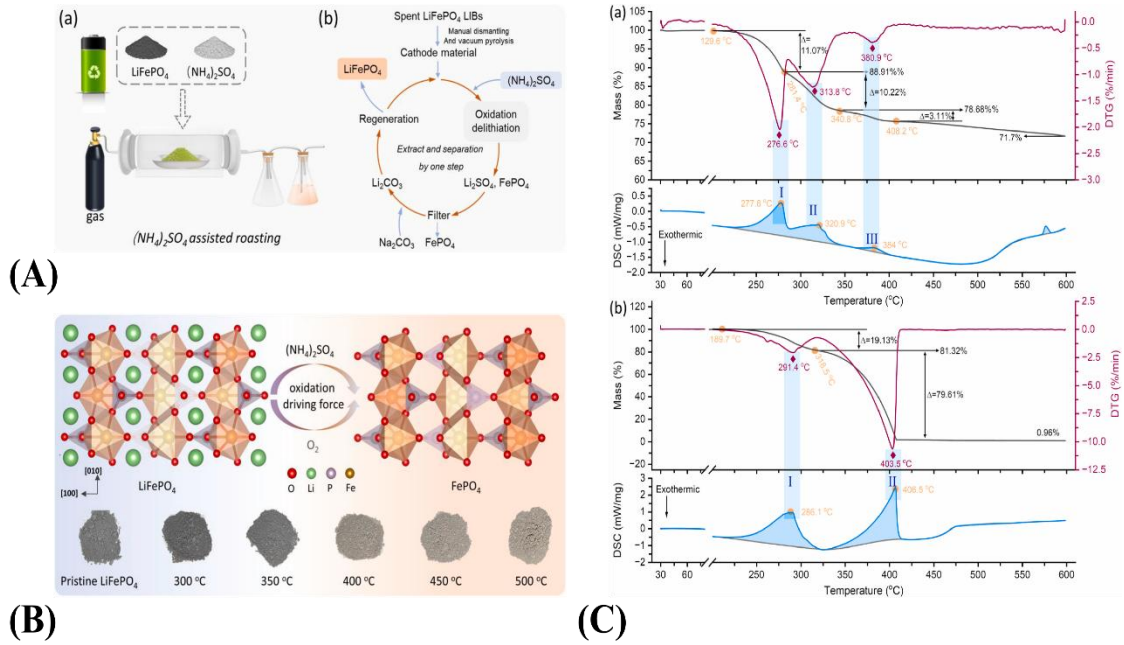

Figure 4 (A) (a) Schematic illustration of the $(NH_4)_2SO_4$ assisted roasting for recycling degraded $LiFePO_4$, (b) the recovery flow sheet of $(NH_4)_2SO_4$ assisted roasting for recycling degraded $LiFePO_4$ [65]. (B) The Schematic illustration of transformation and reaction mechanism under different atmosphere for converting C-LFP to $FePO_4$, the insert digital photo is the sulfation roasting products of C-LFP under different temperature [65]. (C) TG-DSC of the C-LFP and $(NH_4)_2SO_4$ powders under air atmosphere: (a) the mass ratio of C-LFP: $(NH_4)_2SO_4$ = 1: 0.8, (b) pure $(NH_4)_2SO_4$ [65].

In traditional pyrometallurgical SLFP recovery, prolonged high-temperature reactions between raw materials and additives result in substantial energy losses and economic costs during production. Conventional hydrometallurgy imposes greater reagent requirements for leaching processes. Li *et al.* [67] proposed a method for recovering waste lithium iron phosphate using NaOH-assisted low-temperature calcination (**Figure 5(A)**). Under NaOH assistance, Fe(II) in lithium iron phosphate oxidizes to Fe_3O_4 (III) at 150 °C, disrupting the olivine structure. Released Li^+ and Na^+ are captured by PO_4^{3-} forming Li_2NaPO_4 and $LiNa_5(PO_4)_2$. The best process parameters of calcination at 150 °C for 2 h, molar ratio of $LiFePO_4$/NaOH is 1:2, water leaching solid-liquid ratio 1 g/L, produced a best leaching rate of Li of 96.7% (**Figure 5(B)**). Post-calcination products (Fe_3O_4, Li_3PO_4 and Na_3PO_4) separated by water leaching were analyzed by XRD/SEM (**Figure 5(C)**). Water-leached Li_3PO_4 shows rod-like structures (lengths: 1 - 2 μm; diameters: 0.5 μm). Fe_3O_4 particle sizes remain uneven due to precursor influence, but EDS confirms uniform Fe/O distribution. The mechanism of NaOH-assisted calcination depicted in **Figure 5(D)** involves complete encapsulation of $LiFePO_4$ crystals by NaOH during ball milling. Temperature increase breaks Li-O/Fe-O bonds; Fe^{2+} captures OH^- forming $Fe(OH)_2$ intermediates decomposing into FeO and H_2O(g). Under Ar atmosphere, FeO spontaneously decomposes into Fe and Fe_3O_4, with Fe further oxidized by H_2O to form Fe_3O_4(g) and release H_2 for charge balance. In $LiFePO_4$, P-O bond maintains structural stability strongest, capturing cations to form $Li_xNa_y(PO_4)_z$ composite salts (soluble $LiNa_5(PO_4)_2$ and insoluble Li_2NaPO_4). Eqs. (12) - (16) illustrate the process.

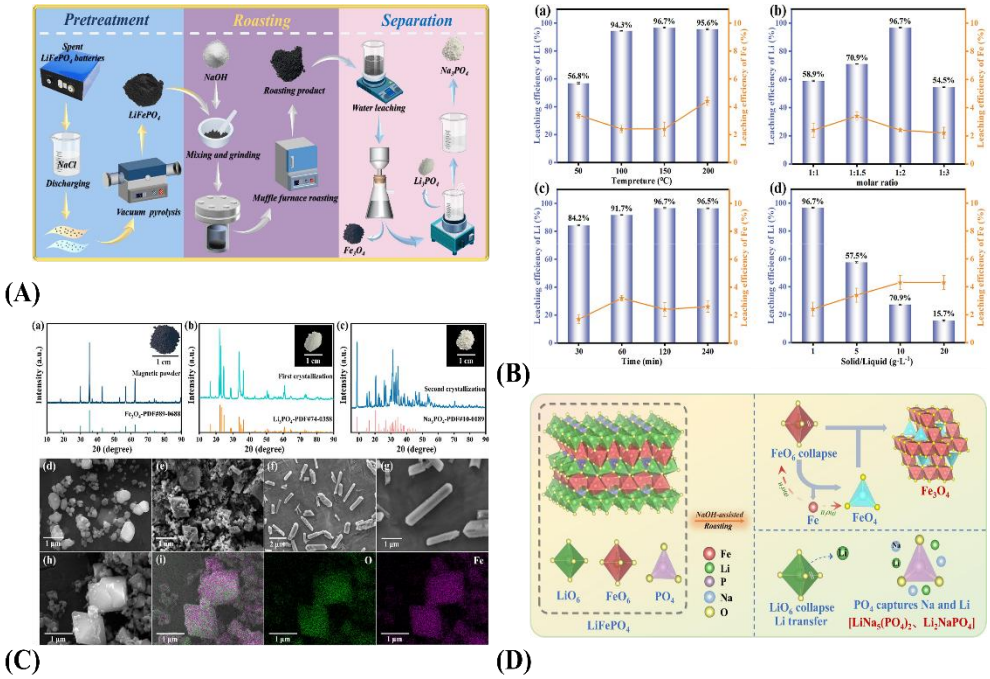

Figure 5 (A) Schematic of the recovery process for spent $LiFePO_4$ batteries [67]. (B) Li and Fe leaching efficiencies for NaOH-assisted roasting at (a) different roasting temperatures, (b) different $LiFePO_4$/NaOH molar ratios, (c) different roasting times and (d) different solid–liquid ratios [67]. (C) XRD patterns and digital photographs of the recovered products: (a) magnetic powders, (b) first crystallization products, and (c) second crystallization products, SEM images of (d) the cathode powders scrapped from cathode sheets, (e) the products obtained from NaOH-assisted roasting, (f) the Li_3PO_4 obtained by stepwise evaporation crystallization, (g) the Li_3PO_4 at high magnification and (h) the Fe_3O_4 after water leaching, (i) EDS mapping images of Fe and O species of the Fe_3O_4 [67]. (D) Conversion mechanism diagram of NaOH-assisted roasting [67].

Formation of intermediate $Fe(OH)_2$

$$3LiFePO_4 + 6NaOH = 3Fe(OH)_2 + LiNa_5(PO_4)_2 + Li_2NaPO_4 \quad (12)$$

Heat decomposition of $Fe(OH)_2$

$$Fe(OH)_2 = FeO + H_2O(g) \quad (13)$$

Disproportionation reaction of FeO

$$4FeO = Fe + Fe_3O_4 \quad (14)$$

Fe oxidized by $H_2O(g)$'

$$3Fe + 4H_2O(g) = Fe_3O_4 + 4H_2 \quad (15)$$

Full reaction

$$3LiFePO_4 + 6NaOH = Fe_3O_4 + LiNa_5(PO_4)_2 + Li2NaPO_4 + 2H_2O(g) + H_2(g) \quad (16)$$

Hu *et al.* [68] proposed an eco-friendly, low-consumption recycling technique as a novel alternative to conventional methods for selective SLFP recovery as shown in **Figure 6 (A)**. This method employs $K_2S_2O_7$ as a roasting aid during low-temperature oxidative atmosphere treatment. Above 378 °C, $K_2S_2O_7$ decomposes into K_2SO_4 and SO_3. Under high-temperature oxygen exposure, SLFP generates Fe_2O_3 while disrupting $LiFePO_4$'s olivine structure, because of the forming $Li_3Fe_2(PO_4)_3$ residues. Carbon content in SLFP facilitates $Li_3Fe_2(PO_4)_3$ reaction with SO_3, producing Li_2SO_4 and $FePO_4$. Li_2SO_4 further reacts with K_2SO_4 to form water-soluble $LiKSO_4$.

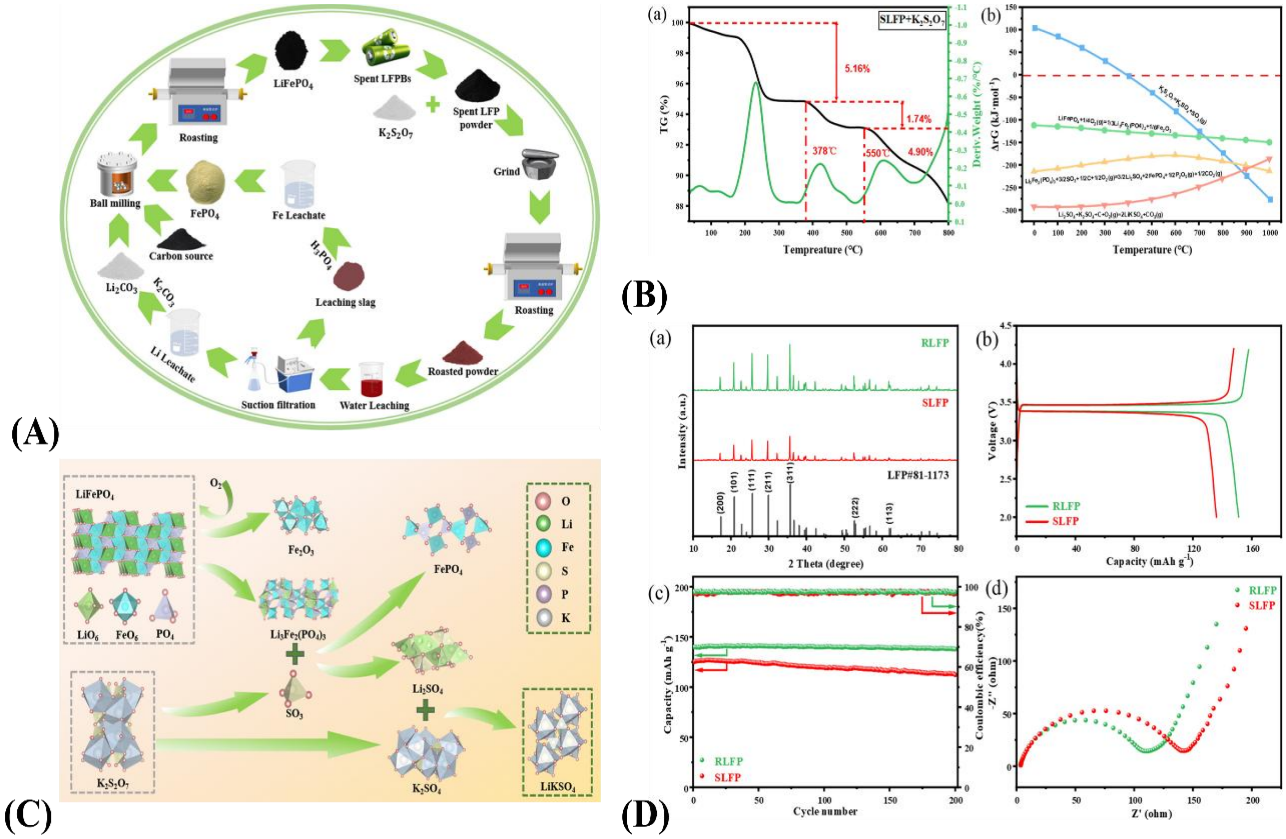

Figure 6 (A) Schematic Representation of the Recycling Strategy for SLFP Cathodes [68]. (B) (a) TG analysis results of mixed materials ($K_2S_2O_7$/SLFP mass ratio = 1.5:1) after grinding; and (b) relationship between temperatures and the Gibbs free energy for the chemical reactions [68]. (C) Conversion mechanism diagram of $K_2S_2O_7$-assisted roasting [68]. (D) (a) XRD patterns of RLFP and SLFP. (b) Initial charge-discharge profiles of RLFP and SLFP at 0.1 C. (c) Cycling stability of the RLFP and SLFP at 1 C. (d) Nyquist plots for SLFP and RLFP [68].

The results of TG analysis of the roasting process and the Gibbs free energy of temperature versus chemical reaction are shown in **Figure 6(B)**. The data indicate that the mass loss process is divided into three stages consistent with the aforementioned reaction process and that the experiment can be carried out spontaneously at high temperatures. The roasting mechanism is shown in **Figure 6(C)**. The whole roasting process reacts as in Eqs. (17) - (21). Water leaching at 60 °C for 30 min followed by saturated K_2CO_3 precipitation yields lithium carbonate, while phosphoric acid treatment recovers $FePO_4 \cdot xH_2O$. Resynthesized $LiFePO_4$ from recycled $FePO_4$, Li_2CO_3, and glucose exhibits 140.06 mAh/g initial capacity with 98.40% retention (137.8 mAh/g) after 200 cycles at 1 C, as shown in **Figure 6(D)**. The pyrometallurgical methods of recovering Li ions are summarized in **Table 2**.

Roasting process

$$K_2S_2O_7 = K_2SO_4 + SO_3(g) \quad (17)$$

$$LiFePO_4 + 1/4O_2(g) = 1/3Li_3Fe_2(PO_4)_3 + 1/6Fe_2O_3 \quad (18)$$

$$Li_3Fe_2(PO_4)_3 + 3/2SO_3 + 1/2C + 1/4O_2(g) = 3/2Li_2SO_4 + 2FePO_4 + 1/2P_2O_5(g) + 1/2CO_2(g) \quad (19)$$

$$Li_2SO_4 + K_2SO_4 + C + O_2(g) = 2LiKSO_4 + CO_2(g) \quad (20)$$

Over all reaction

$$LiFePO_4+1/2K_2S_2O_7+C+5/4O_2(g) = 1/3Fe_2O_3+1/3FePO_4+LiKSO_4+CO_2(g)+1/3P_2O_5(g) \quad (21)$$

Table 2 Recovery of Li by different roasting methods in pyrometallurgy.

Pyrometallurgical	Materials	Conditions	Leaching rate	References
Carbothermal reduction molten	Na_2CO_3, C	Molar ratio: LFP: Na_2CO_3 = 1:1, Molar ratio: LFP: C = 1:2, 900 ℃, 4 h.	Li, > 90%	[64]
Salt-assisted roasting	$(NH_4)_2SO_4$, air	Molar ratio: C-LFP:$(NH_4)_2SO_4$ = 1:0.8, 30 ℃, 10 min.	Li, 97.8%; Fe, < 2%	[65]
	$NaHSO_4$	Mass ratio: $NaHSO_4 \cdot H_2O$/LFP = 1.5, 600 ℃, 1 h; then30 ℃, 1 h.	Li, 98.12%	[66]
	NaOH	Molar ratio of $LiFePO_4$/NaOH is 1:2, solid-liquid ratio is 1 g/L.	Li, 96.7%	[67]
	$K_2S_2O_7$, O_2	The mass ratio of $K_2S_2O_7$ is 150%, 600 °C for 1 h, then 60 °C for 30 min.	Li, -%; Fe-%	[68]

Hydrometallurgical recovery

Hydrometallurgical recovery is the most common and widely used method in SLFP battery recycling. The leaching, enrichment, and separation stages constitute the three core phases of this process. Leaching involves transferring valuable elements from cathode materials into solution, establishing the basis for subsequent enrichment and separation. In cathode material recycling, LFP serves as the primary active substance, with lithium being the principal recoverable metal due to its higher recycling value. In addition, hydrometallurgical recovery of waste lithium iron phosphate can be divided into selective lithium leaching and non-selective lithium leaching based on the results of the main element leaching. However, since most recent studies have focused on selective lithium leaching, this paper will discuss selective leaching. In strongly acidic solutions, the leaching selectivity of lithium and iron in lithium iron phosphate is poor, so selective leaching can generally be achieved by increasing the redox potential through the addition of oxidants. Therefore, the wet leaching process typically employs acidic leaching systems (inorganic or organic) while maintaining LFP's olivine structural stability through the introduction of oxidizing agents to achieve in situ selective lithium extraction.

Inorganic acid leaching

Conventional inorganic acid leaching often involves selective leaching of SLFP cells with various combinations of strong acids paired with oxidizing agents. In which the problem of excessive use of acid is often involved. Li *et al.* [69] proposed a new method to leach the cathode materials of SLFP batteries by using stoichiometric $Na_2S_2O_8$ as the oxidizing agent and low concentration of H_2SO_4 as the leaching agent. The optimal conditions were 0.45 molar ratio of $Na_2S_2O_8$/Li,0.30 M of H_2SO_4, reaction temperature of 60 °C, and reaction time of 1.5 h. The leaching rate of Li^+ was obtained to be 97.53%, that of Fe^{3+} was 1.39%, and that of PO_4^{3-} was 2.58%. Trace amounts of $FePO_4$ in the filtrate were recovered by precipitation by adding $Fe_2(SO_4)_3$ under the condition of keeping the pH at 2.0. The mother liquor was concentrated at 100 °C, and then saturated sodium carbonate solution was added to precipitate Li_2CO_3, and the lithium recovery rate was close to 80%.

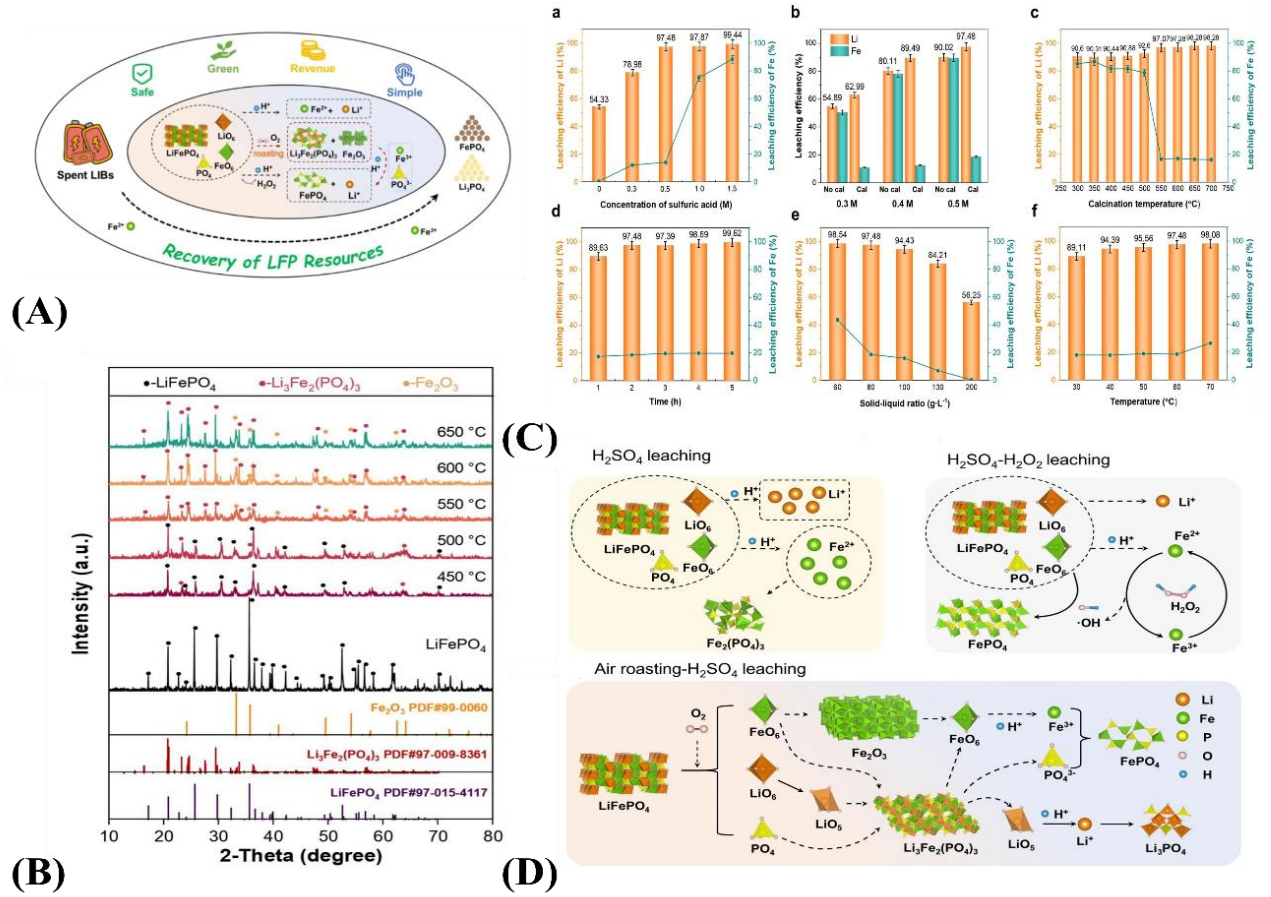

Figure 7 (A) Principles of oxidation in the recovery of SLFP by acid leaching [70]. (B) XRD patterns of products obtained by air roasting at different temperatures in 2 h [70].(C) (a) Leaching efficiency of Li and Fe at different concentrations of H_2SO_4, (b) difference between leaching efficiency of roasted and raw LFP with different concentrations of H_2SO_4,(c) leaching efficiency of Li and Fe of roasted products at different calcination temperature, (d) f leaching efficiency of Li and Fe at different time, solid–liquid ratio and leaching temperature [70]. (D) (a) H_2SO_4 sole leaching reaction mechanism; (b) H_2SO_4–H_2O_2 leaching reaction mechanism; (c) O_2 roasting and acid leaching reaction mechanism [70].

Wang *et al.* [70] revealed the oxidation mechanism of $LiFePO_4$ in air and in solutions containing oxidants such as H_2O_2, and the effect of oxidation on the selective leaching of LFP, as shown in **Figure 7(A)**. The cathode materials of SLFP batteries were roasted under the effect of oxygen in air, in which Fe^{2+} was oxidized to Fe^{3+}. The physical phase of $LiFePO_4$ was changed to $Li_3Fe_2(PO_4)_3$ and Fe_2O_3, and the structure of the LFP peridotite was disrupted. XRDs of the roasted products at different temperatures are shown in **Figure 7(B)**. Then the roasting residue was done leaching in sulfuric acid solution to get unreacted Fe_2O_3 residue and primary filtrate, and finally the pH was adjusted by adding NaOH to precipitate Fe in the form of $FePO_4$. Then vacuum filtration was carried out to obtain the secondary filtrate, and then the filtrate was heated and crystallized to obtain Li_3PO_4, and the recovery rate of lithium could reach 97.48%. The optimum process parameters of oxidative roasting and sulfuric acid impregnation were obtained, and the optimum oxidative acid leaching process parameters were obtained: the concentration of H_2SO_4 was 0.5 M, the roasting temperature was 550 °C, the solid-liquid ratio was 80 g/L, the leaching temperature was 60 °C, and the leaching time was 2 h, as shown in **Figure 7(C)**.

The principle of leaching experiment is shown in **Figure 7(D)**. Compared with H_2SO_4 - H_2O_2, the air oxidation method improves the iron leaching efficiency and reduces the consumption of H_2SO_4 while saving H_2O_2. The difference in iron leaching efficiency was attributed to the different leaching mechanisms of solid-solid and solid-liquid-solid transformations. During

H_2SO_4 leaching without H_2O_2, the acid destroys the structure of LFP and leads to the complete leaching of Li while Fe enters the solution in large quantities, and iron exists in the solution as Fe (II) or $Fe_3(PO_4)_2$-$8H_2O$. Where H^+ directly destroys the FeO_6 octahedra, allowing the LiO_6 octahedra to collapse Li^+ into solution. During the combined H_2O_2/ H_2SO_4 leaching process, the reaction starts with a small amount of H^+ dissolving a small amount of LFP, and then Fe (II) stimulates the decomposition of H_2O_2 to rapidly generate a large amount of -OH with strong oxidizing ability. At the solid-liquid interface, $FePO_4$ is formed immediately from locally high concentrations of Fe (III) and H_3PO_4. Afterwards, -OH directly oxidizes and converts most of the remaining LFP to $FePO_4$, while Li^+ is selectively leached in solution. In the experiments of air oxidation roasting followed by acid leaching, the transformation of part of FeO_6 into Fe_2O_3 during roasting led to vacancies in the LFP structure, causing the LiO_6 octahedra to collapse first to form LiO_5 hexahedra. In the subsequent acid leaching, the vacancies made it easier for H^+ to disrupt the structure of FeO_6, causing it to form Fe (III), which contributed to the further collapse of LiO_5 hexahedra. At the same time, some Fe_2O_3 dissolves in the acidic solution. The dissolved Fe (III) and PO_4^{3-}form $FePO_4$ in solution, a solid-liquid-solid reaction.

Inorganic acid leaching can also use other strong acids as leaching solvents in addition to H_2SO_4 as leaching agent. Dai *et al.* proposed a method to selectively extract lithium from waste LFP by using nitric acid's own oxidizing property, as shown in **Figure 8(A)** [71]. Under the optimal reaction conditions: A HNO_3/Li molar ratio of 2 and a reaction time of 2 h reaction temperature of 120 °C, the lithium leaching efficiency reached 99.5% and the selectivity reached 82.1%, as shown in **Figure 8(B)**. Firstly, LFP was destroyed into Fe^{2+}, Li^+ and H_3PO_4 under acidic solution conditions. Secondly, Fe^{2+} ions were oxidized to form Fe^{3+} under acidic and oxidizing conditions. During the dissociation of $LiFePO_4$ and oxidation of Fe^{2+}, H^+ is consumed, leading to increased pH of the solution. Finally, the combination of iron and phosphorus leads to the precipitation of $FePO_4{\cdot}2H_2O$. After the process of dissolution, oxidation and precipitation of iron in LFP powder, lithium can be selectively leached from spent LFP.

The whole reaction equation is Eqs. (22) - (26). The reaction steps of the whole lithium selective extraction process, including the first step of LFP decomposition, the second step of Fe^{2+} oxidation, and the third step of P and Fe reprecipitation. The results show a theoretical basis for the selective recovery of lithium using nitric acid with the retention of Fe and P in the leaching slag. Scanning electron microscopy and TEM results are shown in **Figure 8(C)**, the SLFP particles have obvious agglomeration, which may be caused by the binder PVDF. Semi-quantitative EDS spectroscopy results showed the presence of Cu, Al and F impurities in SLFP. The low content of impurity elements Cu, Al and F in the leaching slag indicates that the impurity components were effectively removed after the experiment, which is conducive to the subsequent recovery of $FePO_4$ from the leaching slag. The TEM (mapping) results of the solid-phase product showed that the Fe/P/O molar ratio was highly consistent with the theoretical value of $FePO_4{\cdot}2H_2O$, indicating that $FePO_4$ was produced smoothly. The leaching rate of elemental P was maintained at a constant level of about 4.5%. around 4.5%. This phenomenon may be due to an imbalance between P and Fe in the feedstock, resulting in an excess of P with out enough corresponding Fe, which enters the solution to form $FePO_4{\cdot}2H_2O$ precipitation. This imbalance ultimately leads to a decrease in the leaching selectivity of Li. In order to promote the precipitation of P, a certain amount of $Fe(NO_3)_3{\cdot}9H_2O$ was added to the slurry at the beginning of the leaching process to improve the extraction selectivity of Li.

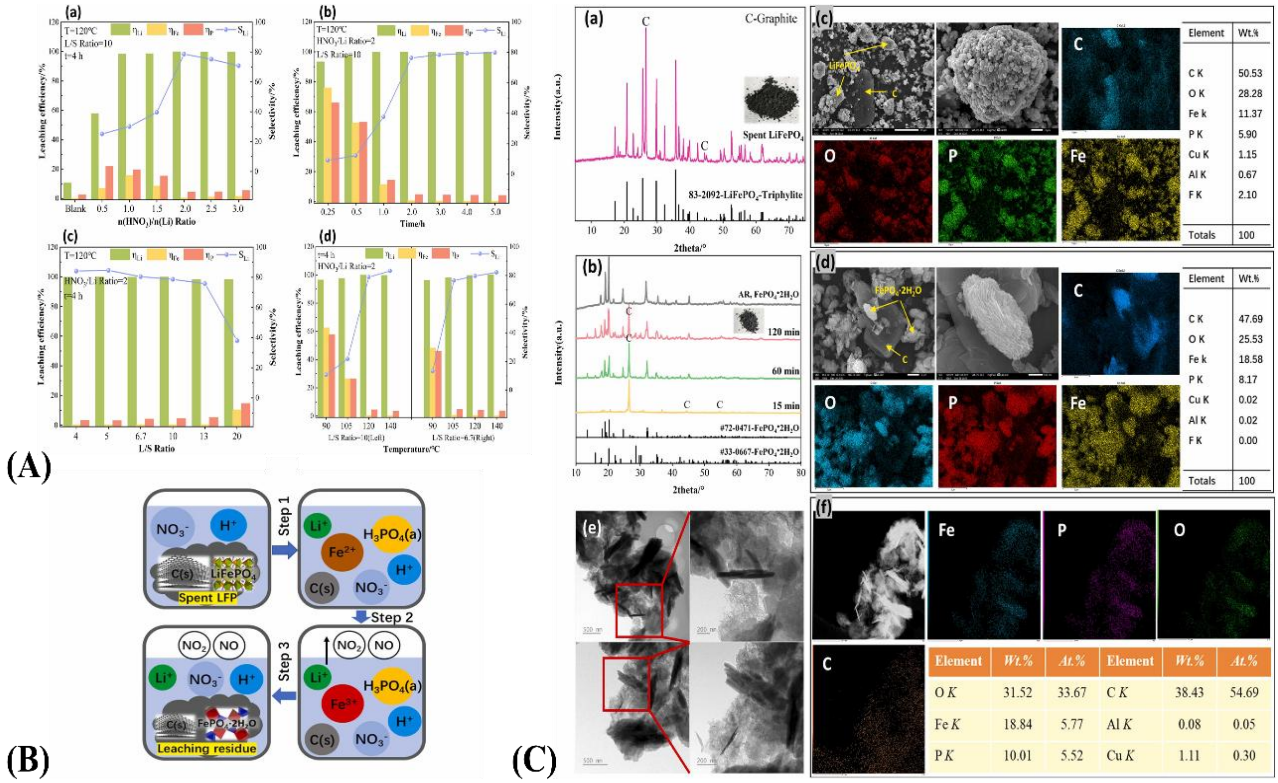

Figure 8 (A) Effects of (a) HNO_3/Li ratio, (b) holding time, (c) L/S ratio, (d) leaching temperature on the selective leaching of Li [71]. (B) process of selective extraction of lithium [71]. (C) XRD patterns of (a) spent LFP and (b) leaching residue, SEM-EDS images of (c) spent LFP (d) and leaching residue, (e) TEM images and (f) elemental mapping images of leaching residue [71].

$$LiFePO_4 + 3H^+ = Fe^{2+} + Li^+ + H_3PO_4(a) \quad (22)$$

$$Fe^{2+} + NO^{3-} + 2H^+ = Fe^{3+} + NO_2(g) + H_2O(l) \quad (23)$$

$$Fe^{3+} + H_3PO_4(a) + 2H_2O(l) = FePO_4{\cdot}2H_2O + 3H^+ \quad (24)$$

$$NO_2(g) + 1/3H_2O(l) = 2/3NO^{3-} + 2/3H^+ + 1/3NO(g) \quad (25)$$

$$LiFePO_4 + 4/3H^+ + 1/3NO^{3-} + 4/3H_2O(l) = FePO_4{\cdot}2H_2O + Li^+ + 1/3NO(g) \quad (26)$$

Liu *et al.* [72] used stoichiometric ratio of hydrochloric acid and sodium hypochlorite as acidic medium and oxidizing agent to recover LFP powder and obtain lithium carbonate product with purity higher than 99.7%, as shown in **Figure 9(A)**. The optimal process conditions were established as 0.6 mol/L HCl, HCl/Li molar ratio of 1.3, ClO_3^-/Li molar ratio of 0.6, temperature of 15 °C, and reaction time of 20 minutes for lithium leaching. The leaching rates of Li and Fe were greater than 95% and less than 0.1%, respectively. And the crystal structure of the powder remained basically unchanged throughout the leaching process, as shown in **Figure 9(B)**.

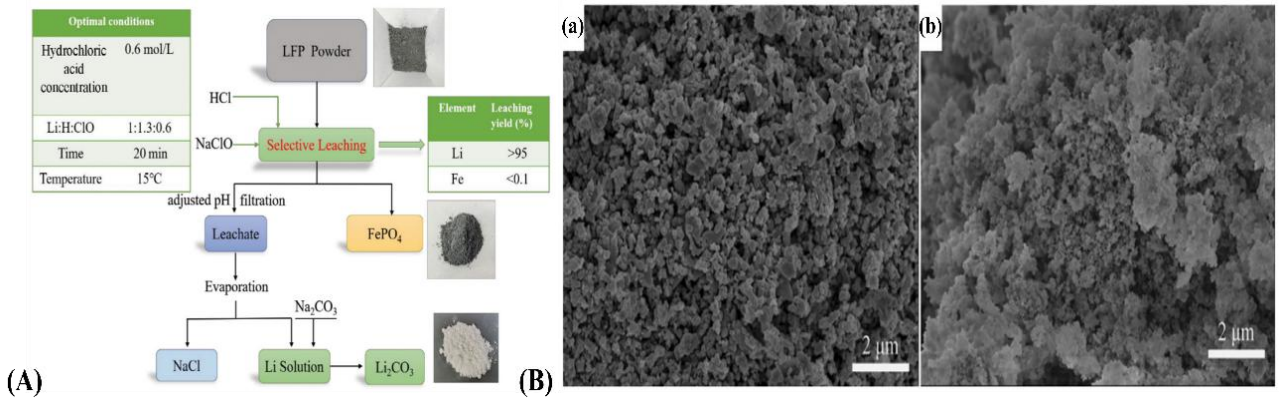

Figure 9 (A) Flow chart of the selective leaching process of Li from a simulation of $LiFePO_4$ powder [72]. (B) Scanning electron microscope (SEM) characterization of (a) $LiFePO_4$ and (b) leaching residue [72].

Organic acid leaching

In the field of SLFP recovery, in addition to the use of inorganic acid leaching to recover SLFP, organic acid can also be used to recover SLFP. Organic acid leaching avoids the problem of excessive use of strong acids and bases in the use of inorganic acid leaching, which is greener and friendlier to the environment. As a green oxidant, hydrogen peroxide (H_2O_2) is widely used in organic acid leaching systems for several reasons: 1) Its strong oxidizing capability rapidly converts Fe^{2+} in the cathode material to Fe^{3+}, which constitutes the fundamental mechanism for the selective leaching of lithium from lithium iron phosphate (LFP) [73-75]. Its reduction products are only water (H_2O) and/or hydroxyl radicals (·OH), thereby avoiding the introduction of foreign anions that could complicate the leaching solution. 3) The leaching process operates efficiently under ambient pressure and at moderate temperatures (50 - 90 °C), significantly lowering energy consumption and equipment demands, in alignment with green chemistry principles [76]. 4) Any residual H_2O_2 decomposes completely into water and oxygen upon heating or catalysis, leaving no harmful residues in the leachate or products. This simplifies subsequent purification and lithium recovery steps, thereby enhancing final product purity [77]. 5) Organic acids are more environmentally benign than mineral acids owing to their biodegradability and lower corrosiveness [78]. The combination of H_2O_2 with organic acids thus constitutes an efficient and eco-friendly leaching system.

Ji *et al.* [79] proposed a new method for selective leaching of lithium and simultaneous separation of lithium, iron, and aluminum by using formic acid as the leaching agent and hydrogen peroxide as the oxidizing agen. As shown in **Figure 10(A)**, compared with the traditional method, this study realized the synchronization of pretreatment with the separation of cathode materials and selective leaching of lithium. The optimal process conditions were established as HCOOH of 0.4 mol/L, H_2O_2 volume fraction of 3.0%, material-liquid ratio of 50 g/L, and reaction at 60 °C for 20 min are shown in **Figure 10(B)**. The leaching rate of Li was 98.84%, and the leaching rate of Fe and Al were both less than 1%. The Eh-pH diagram of the Li-Fe-P-H_2O system showed that the pH was in the range of 1.28 ~ 6.09, $FePO_4$ can be stabilized as a leaching product. The leaching residue $FePO_4$ was simply reduced and roasted under H_2 atmosphere to obtain $Fe_2P_2O_7$, a new type of material that can be used as cathode for lithium-ion batteries, as shown in **Figure 10(C)**. NaOH was added to the filtered lithium solution to remove a small amount of impurities and adjust the pH 9-10, and then the filtrate was heated to evaporate the aqueous method, and finally an excess of Na_3PO_4 was introduced to form a white precipitate, which recovered lithium in the form of Li_3PO_4. As shown in **Figure 10(D)**, the regenerated material was tested for ultra-long cycling performance at 1 ag^{-1} and still provided a stable capacity of 147.2 mA h g^{-1}, with a capacity retention rate of 88.55% calculated from the 5th to the 500th cycle.

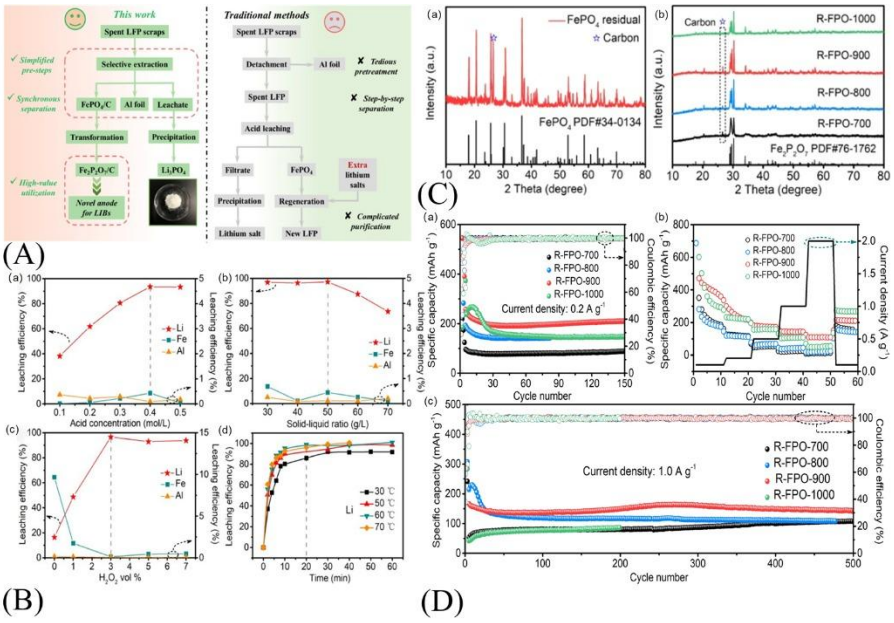

Figure 10 (A) The proposed recovery flow chart in this study compared with traditional methods [79]. (B) Effects of (a) acid leaching, (b) solid-liquid ratio, (c) amount of H_2O_2, and (d) time and temperature on the leaching efficiencies of Li, Fe and Al from spent LFP cathode scraps [79]. (C) XRD patterns of (a) the leaching residue and (b) the regenerated materials obtained at different temperatures [79]. (D) (a) cycle performance at 0.2 Ag^{-1}, (b) rate capability and (c) long term cycling performance at 1 Ag^{-1} of different samples [79].

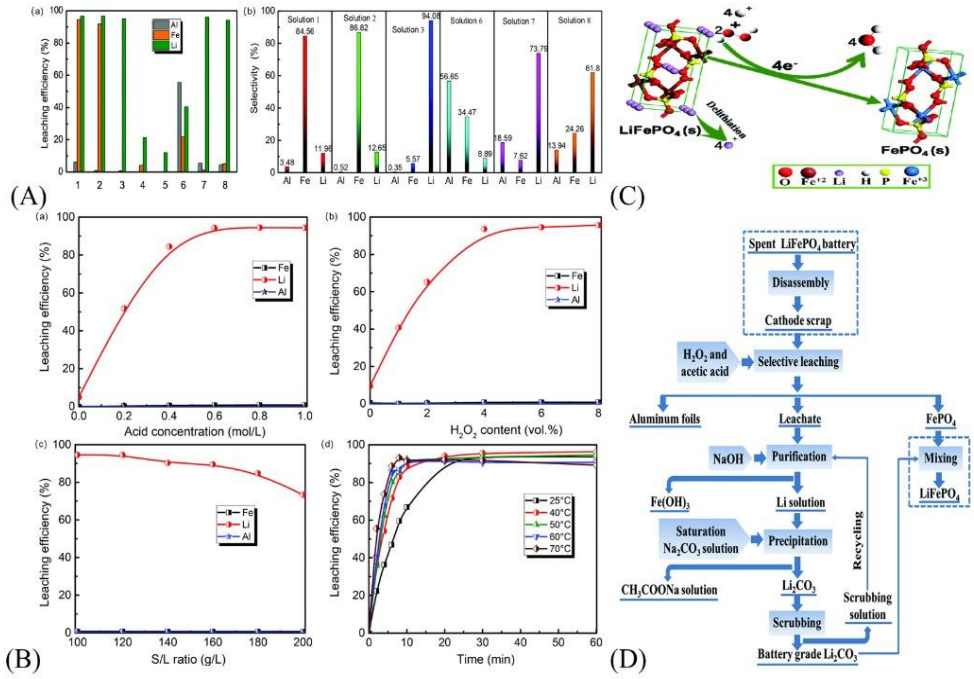

Figure 11 (A) (a) Leaching efficiency of metals employing different leaching solu-tions. 1. Oxalic acid with H_2O_2; 2. citric acid with H_2O_2; 3. acetic acid with H_2O_2; 4. acetic acid; 5. H_2O_2; 6. HCl with H_2O_2; 7. H_2SO_4 with H_2O_2; 8. HNO_3 with H_2O_2, (b) Selectivity of leached metals into different leaching solutions [80]. (B) Effects of (a) acid concentration, (b) H_2O_2 content (vol%), (c) solid-to-liquid ratio, (d) leaching times on the leaching efficiencies of Li, Fe and Al from spent LFP cathode scraps [80]. (C) The products of the leaching reaction process of spent $LiFePO_4$ with acetic acid in the presence of H_2O_2 [80]. (D) A proposed green process for the recycling of valuable metals from the spent $LiFePO_4$ cathode scrap [80].

Yang *et al.* [80] proposed a method for efficient and sustainable selective leaching of SLFP using acetic acid and hydrogen peroxide. They also investigated the selectivity of different solutions toward major elements and impurities in SLFP, as shown in **Figure 11(A)**. Results indicate acetic acid solution exhibits higher selectivity for lithium compared to three major inorganic strong acids during leaching while causing less dissolution of aluminum and iron. This suggests the combination of acetic acid and hydrogen peroxide can effectively leach lithium from SLFP. Under the optimal conditions of 0.8 mol/L CH_3COOH, 6.0 vol% H_2O_2, 120 g/L solid-liquid ratio, 50 °C, and 30 min, the lithium leaching rate reached 95.05% (**Figure 11(B)**). Reactions during leaching are depicted in Eqs. (27) - (29). Based on the E-pH diagram of Li-Fe-P-H_2O system, when electrochemical potential exceeds 0.56 V, $FePO_4$ phase remains stable at pH 0.1 - 7.2. During leaching, SLFP undergoes in situ electron transfer from Fe(II) to Fe(III) with crystal distortion triggering delithiation, where protons and oxidants promote this process. The selective recovery principle is shown in **Figure 11(C)** Researchers also proposed a green closed-loop recovery process (**Figure 11(D)**), achieving Al, Fe, Li recovery rates of 99.47%, 99.07%, and 84.76% respectively. This process utilizes the synergy between the oxidizing capability of H_2O_2 and the moderate acidity of CH_3COOH to enable precise selective extraction of lithium from $LiFePO_4$, while simultaneously stabilizing iron within the $FePO_4$ crystal lattice [73-75]. A closed-loop material flow design ensures the conversion of all by-products (Al foil, $FePO_4$, CH_3COONa) into valuable products and allows for the recycling of process water. This approach effectively eliminates secondary waste and effluent generation at both the source and the end of the process.

$$H_2O_2 + 2H^+ + 2e^- = H_2O \qquad E_1^\theta = 1.77\ V \tag{27}$$

$$CH_3COOH(aq) \rightarrow CH_3COO^-(aq) + H^+ \qquad pK_a = 4.75 \tag{28}$$

$$LiFePO_4(II)(s) + CH_3COOH(aq) + 1/2H_2O_2(aq) \rightarrow FePO_4(III)(s) + CH_3COO^-(aq) + Li^+(aq) + H_2O(l) \tag{29}$$

The presence of a large number of natural organic acids also presents additional possibilities for the recycling of spent iron phosphate batteries [81]. Fan *et al*. proposed a new method for the selective recovery of lithium by mechanically assisted mixed grinding of SLFP with oxalic acid followed by aqueous leaching treatment, as shown in **Figure 12(A)** [82]. The optimal process conditions were established as a grinding speed of 500 rpm, a grinding time of 2 h, and a molar ratio of SLFP to oxalic acid of 20:1. The leaching rate of lithium was 99%, and 94% of iron was simultaneously recovered in the form of FeC_2O_4-$2H_2O$. The structure of LFP was disrupted in the mechanochemical process. The mechanism of the chemical reaction occurring in the mechanically assisted grinding process is shown in **Figure 12(B)**, where the particle size of the material decreases under the action of mechanical force, and the increase of the local temperature facilitates the occurrence of the new reaction. The chemical reaction equation for the mechanically assisted grinding process is Eq. (30), and thermodynamic analysis shows that the ΔrGm^θ of the reaction is −112.545 kJ/mol, which is a spontaneous reaction at room temperature.

$$LiFePO_4 + 1/2H_2C_2O_4 \rightarrow 1/2FeC_2O_4 + Li^+ + 1/2Fe^{2+} + PO_4^{3-} + H^+ \tag{30}$$

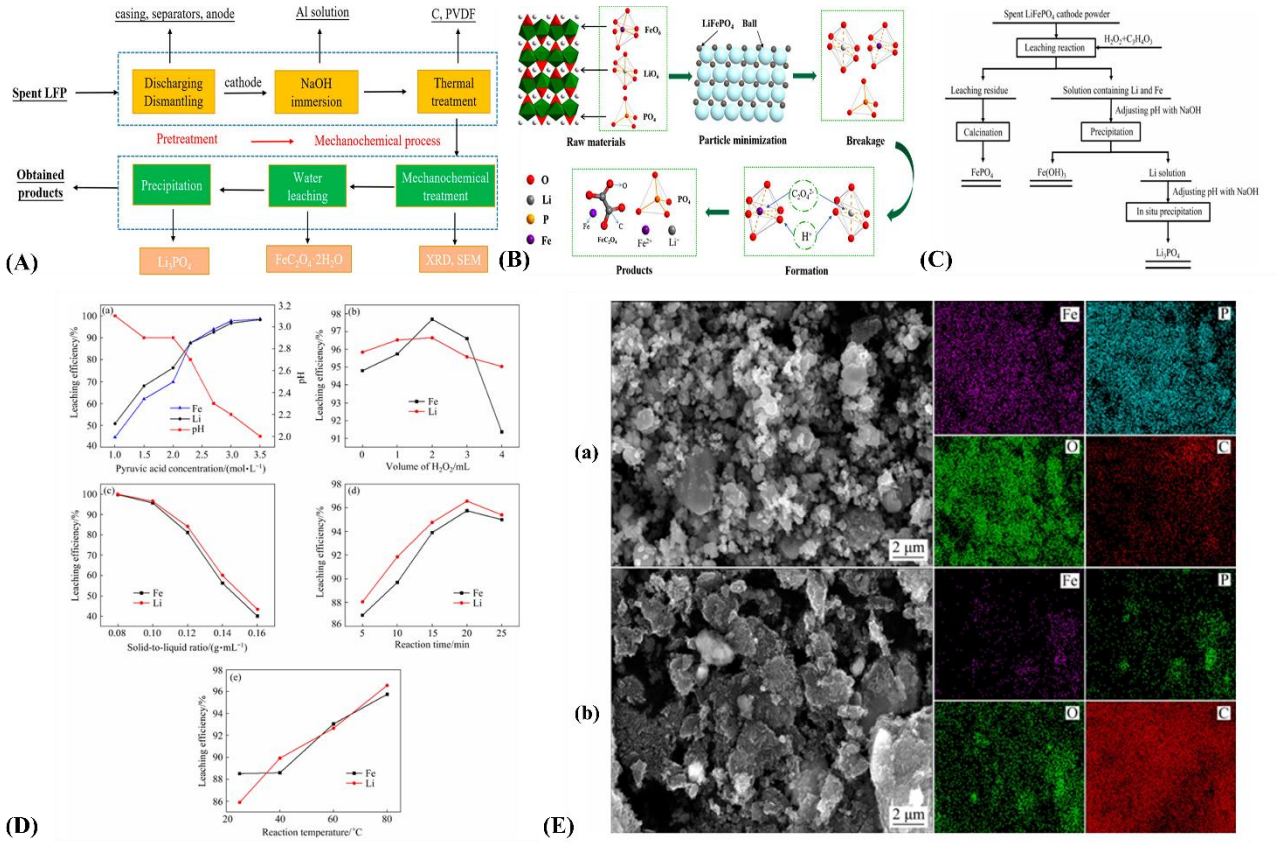

Figure 12 (A) Mechanochemical activation process for spent $LiFePO_4$ batteries recycling [82]. (B) Possible products and mechanism in the mechanochemical process [82]. (C) Process flow of recovering valuable metal from spent $LiFePO_4$ cathode powder [83]. (D) Effects of different process parameters on leaching efficiency of spent $LiFePO_4$ cathode powder: (a) Pyruvic acid concentration; (b) Hydrogen peroxide volume; (c) Solid-to-liquid ratio; (d) Reaction time; (e) Reaction temperature[83]. (E) FE-SEM images and element mappings of spent cathode before (a) and after (b) leaching [83].

Wang *et al.* [83] proposed pyruvic acid as the leaching agent and H_2O_2 as the oxidizing agent as shown in **Figure 12(C)** and explored the optimal process parameters. Finally, lithium was recovered from the leach solution by in situ precipitation to obtain Li_3PO_4 final product with a purity of 96.5 wt%. **Figure 12(D)** shows that the best immersion process parameter of pyruvic acid concentration of 3.0 mol/L, H_2O_2 volume of 2 mL, material-liquid ratio of 0.1 g/mL, and leaching at 80 °C for 20 min. The chemical reaction equation for the whole leaching process is shown in Eq. (31), where Fe^{2+} in LFP is oxidized to Fe^{3+} and leached as $FePO_4$. The $\Delta rG^{\theta} = -73.89$ kJ/mol of the reaction process, and the reaction proceeded spontaneously. The microscopic morphology of the SLFP cathode material was similar to that of the pyruvic acid leaching slag, which was characterized by larger particles, and thus a large amount of carbon remained in the leaching slag, as shown in **Figure 12(E)**. To address this phenomenon, it will be necessary to calcine the leaching slag at 600 °C for 4 h to remove the C-containing impurities.

$$CH_3COCOOH + LiFePO_4 + 1/2H_2O_2 \rightarrow CH_3COCOO^- + Li^+ + FePO_4 + H_2O \quad (31)$$

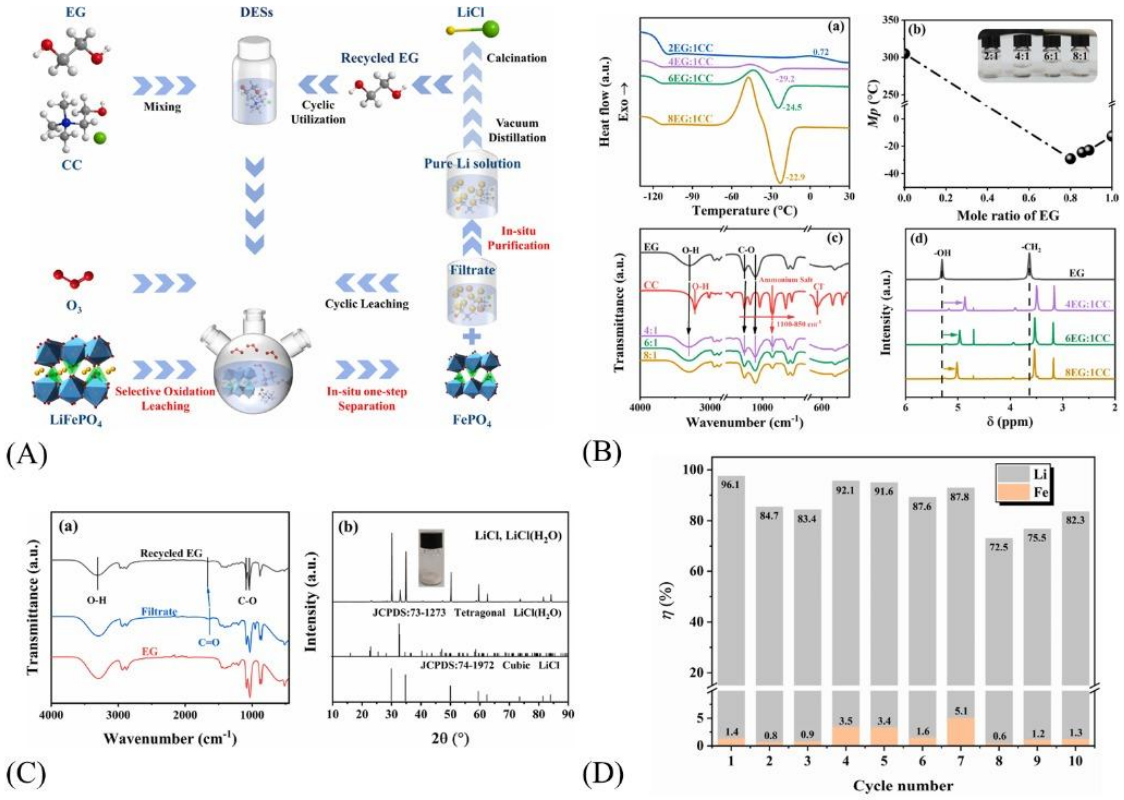

Figure 13 (A) The flowsheet of recovering Li from spent LIBs cathode active material ($LiFePO_4$) [86]. (B) (a) DSC curves, (b) binary phase diagram of DESs with different MEG:CC; (c) FTIR spectra and 1H NMR spectra of pure EG, CC and corresponding DESs. Inset in (B): digital photos of DESs with different MEG:CC at room temperature for a period of time [86]. (C) (a) FTIR spectrum of as-recycled EG, filtrate and pure reagent EG, (b) XRD pattern of as-obtained product [86]. (D) ηLi and ηFe at ten cycles under the optimum conditions (6 h, 20 g/L, 8EG:1CC, 40 °C) [86].

Conventional hydrometallurgical processes for spent lithium iron phosphate (SLFP) recovery typically rely on inorganic strong acids or organic acids supplemented with chemical oxidants to break down the stable olivine structure and oxidize Fe^{2+}, enabling selective lithium leaching [29]. These methods, however, inevitably produce large volumes of acidic wastewater and potentially harmful by-products. Deep eutectic solvents (DESs), a novel class of green solvents composed of hydrogen bond donors (e.g., carboxylic acids, alcohols) and acceptors (e.g., quaternary ammonium salts), offer a promising alternative [84]. While DESs can dissolve metal oxides and avoid generating intractable wastewater, and have been explored for recycling spent ternary batteries, their inherent composition often includes substantial reducing agents (e.g., carboxylic acids, amides, alcohols), which hinders the creation of the oxidizing environment necessary for selective LFP leaching. Consequently, research on DES application for LFP recovery remains limited, despite the solvents' generally excellent biodegradability and low toxicity, and the potential for solvent recovery and reuse via evaporation and concentration [85].

A groundbreaking study by Tang et al. introduced a synergistic leaching system using a low-melting-point DES (ethylene glycol/choline chloride, EG:CC) combined with ozone (O_3), which provides a highly promising green pathway for SLFP recycling [86]. This system achieved highly efficient selective lithium recovery (ηLi ≥ 92.2%) with minimal iron dissolution (ηFe ≤ 1.6%), as depicted in **Figure 13(A)**. The deep eutectic solvent (DES) composed of ethylene glycol (EG) and choline chloride (CC) offers advantages including low toxicity, biodegradability, and low vapor pressure, and the overall process eliminates the need for direct addition of acidic reagents. In this system, ozone first oxidizes EG to generate oxalic acid, which supplies the necessary protons for the leaching reaction. The ozone then further oxidizes Fe^{2+} to Fe^{3+} as the leaching proceeds. Detailed

characterization of its physicochemical properties, such as low viscosity (which enhances mass transfer) and a hydrogen-bond-stabilized liquid structure (**Figure 13(B)**), confirms its potential as a green leaching medium. The use of ozone (O_3) as the oxidant is crucial due to its high redox potential (E^0 = 2.076 V), which is far more effective than O_2, and it introduces no anionic impurities. After leaching, iron remains as stable $FePO_4$, a direct precursor for cathode material resynthesis. Trace dissolved Fe^{3+}, which has low solubility in the DES, can be precipitated as $FePO_4 \cdot 3H_2O$ by simple heating (150 °C), bypassing the alkali-intensive pH adjustment steps of traditional processes. Notably, the primary DES component, ethylene glycol (EG), can be recovered via vacuum distillation with an efficiency of up to 95%, and the recovered EG shows FTIR spectra nearly identical to the pure reagent (**Figure 13(C)**). The system also demonstrated excellent recyclability, maintaining an average lithium leaching efficiency of 85.4% and an iron leaching rate of 2.0% over 10 cycles (**Figure 13(D)**).

Table 3 Some types of blended cathode materials related to $LiFePO_4$.

No	Cathode	Advantages	References
1	Blends of $LiFePO_4$ with $Li[Li_{0.17}Mn_{0.58}Ni_{0.25}]O_2$	Low cost, safety and high charge discharge rate	[89]
2	$xLi_2MnO_3(1\text{-}x)LiMO_2$ and $LiFePO_4$	High power capability and thermal stability	[90]
3	Blends of $LiFePO_4$ with $Li_3V_2(PO_4)_3$	Control capacity loss	[91]
4	Coating $LiNi_{0.5}Co_{0.2}Mn_{0.3}O_2$ with $LiFePO_4$	Enhancedcapacity retention and long life	[92]

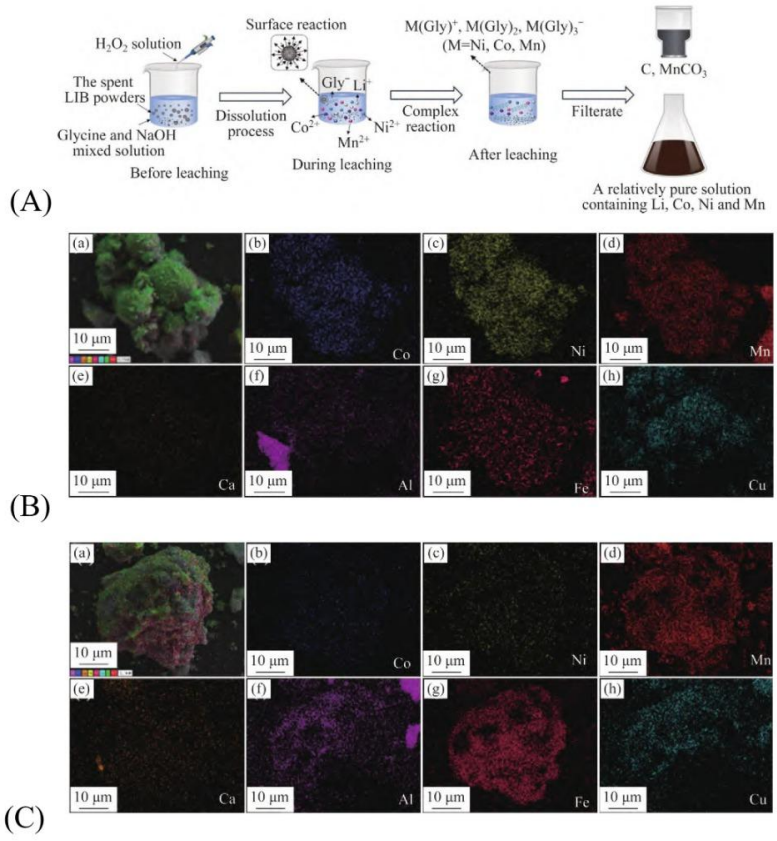

Figure 14 (A) Leaching mechanism of the spent LIBs powder in the alkaline glycinate system [93]. (B) EDS analysis of raw materials for decommissioned lithium-ion batteries [93]. (C) EDS analysis of leaching residue after leaching experiments [93].

Lithium iron phosphate (LFP) and ternary materials (e.g., NCM) are the dominant cathode chemistries in the electric vehicle market. They present a performance trade-off: LFP offers superior cycling stability but limited rate capability, whereas NCM provides high energy density at the expense of safety [87,88]. Blending these materials is a promising strategy to develop advanced power batteries, as summarized in **Table 3**, making the recycling of such hybrid waste streams imperative [89-92]. A central challenge in this recycling process is achieving selective leaching of valuable metals (e.g., Li, Ni, Co, Mn) while effectively suppressing the dissolution of iron from LFP and aluminum from the current collector foil, which is crucial for obtaining a pure leachate and simplifying downstream purification.

Dou *et al.* [93] have proposed a highly selective green leaching process using an alkaline glycinate system to address this challenge. Their method achieves efficient leaching of valuable metals (Li, Co, Ni, Mn) while strongly inhibiting the dissolution of Fe and Al impurities. The proposed mechanism, illustrated in **Figure 14(A)**, involves synergistic reduction by H_2O_2 and coordination by glycinate anions (Gly^-). Under optimal conditions (3 mol/L Gly, pH 8, 90 °C, 5 vol.% H_2O_2, 3 h), leaching efficiencies for Li, Co, and Ni reached 96.31%, 83.18%, and 91.56%, respectively, while the concentrations of Fe and Al in the leachate were suppressed to merely 53.56 mg/L and 46.13 mg/L. This high selectivity originates from the differential complexation behavior of Gly^-: It forms stable aqueous complexes with Co^{2+}, Ni^{2+}, and Mn^{2+}, while iron remains encapsulated in unreacted $LiFePO_4/FePO_4$ or forms stable precipitates, and aluminum is passivated by its surface oxide layer in the alkaline medium. EDS analysis of the raw material and the leaching residue (**Figures 14(B)** and **14(C)**) shows that the valuable metal phases have been effectively removed, whereas the impurity phases containing Fe and Al remain largely intact. This result confirms the exceptional phase-level selectivity of the leaching system. **Table 4** summarizes the different methods of hydrometallurgical recovery of SLFP.

Table 4 Different leaching methods of hydrometallurgical Li.

Hydrometallurgical	Materials	Conditions	Leaching rate	References
Inorganic acid	H_2SO_4, $Na_2S_2O_8$	0.3mol/L H_2SO_4, molar ratio: $Na_2S_2O_8$/Li = 0.45, 60 ℃, 1.5 h.	Li, 97.53%; Fe, 1.39%	[75]
	H_2SO_4, H_2O_2	Roasting temperature 500 ℃, 0.50 mol/L H_2SO_4, S/L = 80g/L, 60 ℃, 2 h.	Li, 97.48%	[76]
	HNO_3	Molar ratio: HNO_3/Li = 2, 120 ℃, 2 h.	Li, 99.5%	[77]
	HCL, NaCLO	0.6 mol/L HCl, molar ratio: HCl/Li = 1.3, molar ratio: ClO/Li = 0.6, 15 °C, 20 min.	Li, > 95%; Fe, < 0.1%	[78]
Organic acid	HCOOH, H_2O_2	0.4mol/L HCOOH, 3% H_2O_2, S/L = 50g/L, 60 ℃, 20 min.	Li, 98.84%; Fe, < 1%	[79]
	CH_3COOH, H_2O_2	0.8 mol/L CH_3COOH, 6.0 vol% H_2O_2, solid-liquid ratio 120 g/L, 50 °C, 30 min.	Li, 95.05%	[80]
	$H_2C_2O_4$	A grinding speed of 500 rpm, a grinding time of 2 h, molar ratio:SLFP:oxalic acid = 20:1.	Li, 99%; Fe, 94%	[82]

Hydrometallurgical	Materials	Conditions	Leaching rate	References
	$CH_3COCOOH$, H_2O_2	3.0 mol/L $CH_3COCOOH$, 2 mL H_2O_2, S/L = 0.1g/mL, 80 ℃, 20min.	Li, 96.5%	[83]
	EG/choline chloride	20 g/L, 8EG:1CC, 6 h 40 ℃.	Li, 94.7%	[86]
	H_2O_2/ glycinate anions	3 mol/L Gly, pH 8, 90 ℃, 5 vol.% H_2O_2, 3 h	Li, 96.31%	[93]

Direct recycling

During the long-term use of lithium iron phosphate batteries, the charging and discharging processes are most likely to cause capacity loss. In this continuous charge-discharge cycle, lithium ions are lost, and the deintercalated lithium ions cannot return to the main body of the cathode material, resulting in a large number of lithium vacancies in the cathode material and the destruction of the lithium-ion crystal structure. This constitutes the primary cause of lithium-ion battery failure. Lithium iron phosphate materials can be effectively regenerated through elemental compensation and structural repair processes. Direct regeneration technology involves physically disassembling battery components and applying elemental compensation and structural repair processes to restore material performance without disrupting the cathode crystal phase. The focus of research lies in the form of lithium supplementation and the effective insertion of lithium ions. Currently, the primary methods of direct regeneration include high-temperature solid-phase regeneration, hydro/solvent-thermal regeneration, and electrochemical regeneration.

Solid phase sintering

Since the LFP materials directly regenerated by solid-phase sintering have the defects of lower purity and poor performance, Song *et al.* proposed a method to solid-phase regenerate LFP by adding Li_2CO_3, activated carbon nanotubes (CNTs) and glucose [94]. Activated carbon nanotubes were obtained by oxidative calcination and debinding of carbon nanotubes under air conditions, followed by hydroxylation and carboxylation in concentrated nitric acid. In the subsequent high-temperature regeneration process, the three-dimensional conductive network composed of CNTs improves the electrical conductivity and ion diffusion coefficient of the repaired LFPs, which makes the carbon-coated structure more stable. The regeneration enhancement process of the material is shown in **Figure 15(A)**. As shown in **Figure 15(B)**, a comparison of the electrochemical performance of the regenerated LFP (R-LFP) material with that of the new LFP (N-LFP) material indicated that the R-LFP had an excellent specific capacity of 155.47 mA h/g at 0.05 C, which is about 99% of that of the N-LFP. It produced 130.76 mA h/g at 1C multiplication. After 800 cycles, the capacity retention of the cell capacity was 70.84% of 1 C. Scanning electron microscopy analysis is shown in **Figure 15(C)**, the R-LFP material particles are uniform, and its micro-morphology is consistent with the N-LFP morphology. And as far as the results are concerned, the residual PVDF component was carbonized during the heat treatment, which solved the problem of particle agglomeration of the material. The CNTs provided a C source during the solid-phase regeneration of the SLFP material, thus controlling the growth and aggregation of the C-coated $LiFePO_4$ material. The study also assessed the cost of recycling one ton of lithium iron phosphate (LFP), accounting for energy consumption during heating and the depletion of key materials (lithium salts, cathode materials, and reducing agents), as shown in **Table 5**. Calculations indicate that recycling one ton of lithium iron phosphate requires 0.172 tons of standard coal, 0.064 tons of lithium carbonate, 0.15 tons of glucose, and 0.05 tons of carbon nanotubes. Based on market prices, the total cost of these primary consumables amounts to 7,388 $. Compared to the price of virgin LFP (23,254 $ per ton according to 2022 statistics from Shanghai Metal Market), this represents only 33.7% of the cost of new materials.

Table 5 The main consumption costs for regenerating one ton of W-LFP.

Item	Price (Dollar/ton)	Usage (ton)	Costs Dollar
CNTS	59,815	0.05	2.990
Li_2CO_3	67,816	0.064	4,340
Glucose	284	0.15	42
Energy (standard coal)	95	0.172	16
Total	/	/	7,388

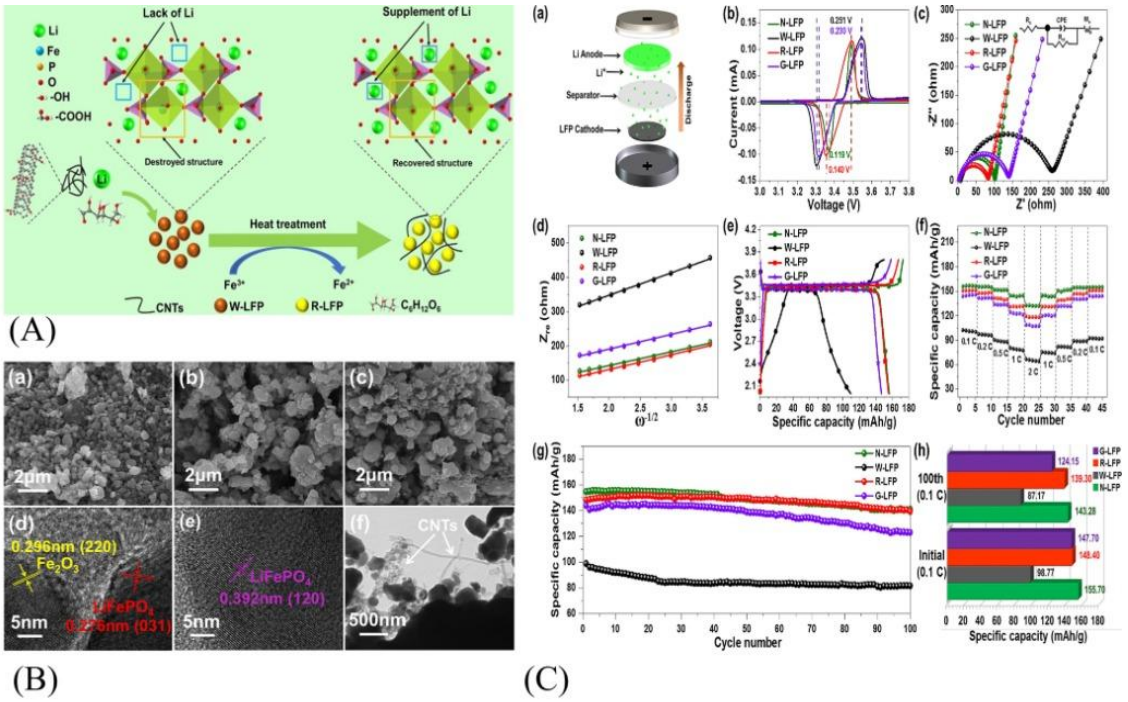

Figure 15 (A) Schematic illustration of the regeneration process of W-LFP [94]. (B) (a) SEM image of W-LFP, (b) SEM image of N-LFP, (c) SEM image of R-LFP, (d) HR-TEM image of W-LFP, (e) HR-TEM image of R-LFP, (f) TEM image of R-LFP [94]. (C) (a) The configuration of lithium half-cell. (b) CV curves of N-LFP, W-LFP, R-LFP and G-LFP, (c) EIS spectra of N-LFP, W-LFP, R-LFP and G-LFP with the equivalent circuit. (d) The relationship between Z' and ω−1/2 in a low frequency region of N-LFP, W-LFP, R-LFP and G-LFP, (e) Charge/discharge profiles at 0.05 C of N-LFP, W-LFP, R-LFP and G-LFP. (f) Rate performance at different current densities of N-LFP, W-LFP, R-LFP and G-LFP, (g) Cycling performance at 0.1 C of N-LFP, W-LFP, R-LFP and G-LFP, (h) Discharge specific capacity retentions at 0.1 C of N-LFP, W-LFP, R-LFP and G-LFP [94].

Direct regeneration of recycled SLFP has a promising application, but there will be irreversible structural and impurity resistance against the feedstock structure throughout the recycling process. Han *et al.* [95] proposed a new method of separating SLFP by first treatment using methanol-citric acid, and then remediation and regeneration of the separated LFP by the remaining PVDF. A solvent mixture of methanol-citric acid was utilized to achieve nondestructive separation of used electrode sheets into SLFP and non-corrosive aluminum foil at room temperature. The SLFP was then calcined by mixing with Li_2CO_3 and PVDF using simple ball milling to obtain regenerated LFP with uniform particle size. The regenerated LFP had a good discharge capacity of 141.5 mA h/g and a discharge retention rate of 99.6% after 100 cycles.

Hydro/solvent-thermal regeneration

High-temperature solid-phase sintering may lead to agglomeration of regenerated LFP material particles due to insufficient contact between the added lithium source and SLFP. The water/solvent-thermal regeneration technique allows the lithium source to be in full contact with the SLFP material in solution, and then the SLFP powder can be repaired by hydrothermal or solvent-thermal reaction, which can effectively solve the problem of non-uniformity of the particles of the cathode material obtained from the regeneration of the solid-phase sintering.

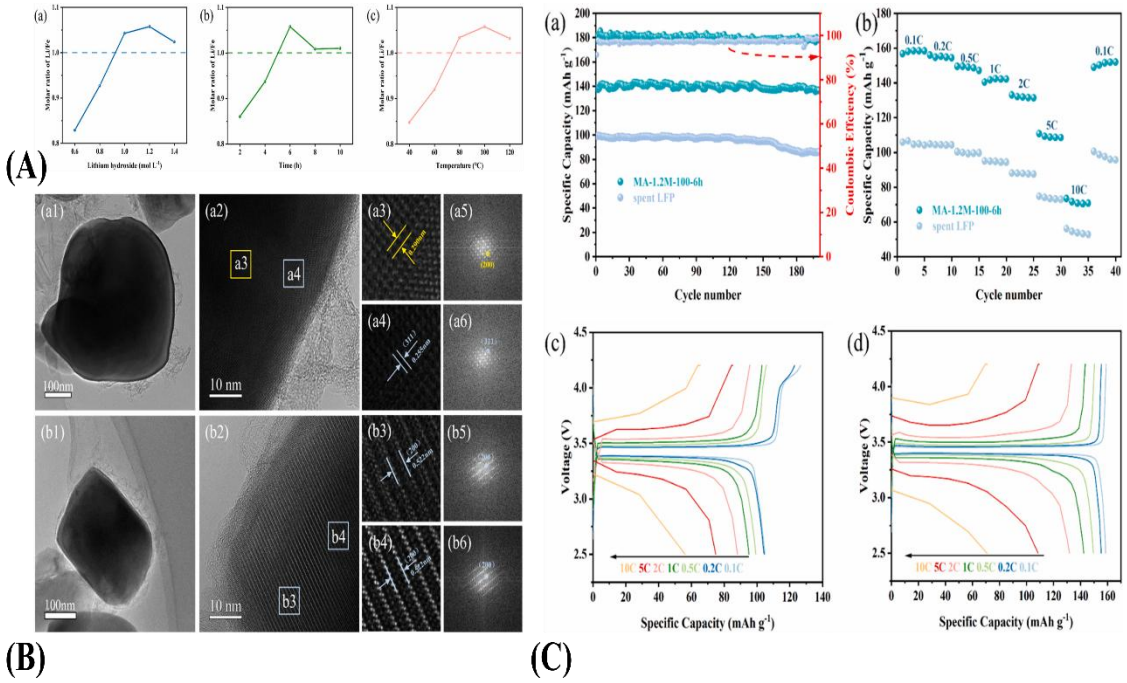

Figure 16 (A) The molar ratio of Li/Fe of regenerated $LiFePO_4$ at different (a) Li concentrations, (b) time and (c) temperature (fixed conditions: pH = 6.0 and a: 100 °C, 6 h; b: Li^+ = 1.2 M, 100 °C; c: Li^+ = 1.2 M, 6 h) [96]. (B) HRTEM images of spent LFP (a1 - a4) and MA-1.2M-100-6 h (b1-b4); the FFT pattern of spent LFP (a5-a6) and MA-1.2M-100-6 h (b5-b6) [96]. (C) Cyclic performance of the spent LFP and Regenerated LFP at different (a) Cyclic performance of spent LFP and MA-1.2M-100-6 h at 1 C rate, (b) rate performance of spent LFP and MA-1.2M-100-6 h. The first charge and discharge curves of the sample at different rates: (c) spent LFP, (d) MA-1.2M-100-6 h [96].

Yang *et al.* [96] proposed a one-step hydrothermal regeneration of LFP materials using $LiOH{\cdot}H_2O$ as a lithium source and dl-malic acid as a reducing agent. SLFP with appropriate amounts of $LiOH{\cdot}H_2O$ and dl-malic acid were added to the hydrothermal reactor and the pH of the mixed solution was adjusted to 6.0. The hydrothermal reaction device was placed on a magnetic stirrer to mix well and then put into a constant temperature blast furnace to regenerate the LFP material. The optimal process parameters for the hydrothermal treatment were lithium-ion concentration of 1.2 mol/L, hydrothermal time of 6 h, and hydrothermal temperature of 100 °C, as shown in **Figure 16(A)**. The scanning electron microscopy of the LFP material is shown in **Figure 16(B)**. The results show that the hydrothermally regenerated material attenuates the problem of SLFP particle size inconsistency and obvious aggregation, and displays excellent particle dispersion. HRTEM of the regenerated material after annealing at 650 °C was tested. There is a 0.290 nm $FePO_4$ lattice stripe in the SLFP material, corresponding to the (200) crystal plane of $FePO_4$. In contrast, only the (200) crystal plane of $LiFePO_4$ was observed in the regenerated material, which corresponds to a crystal plane spacing of 0.522 nm. The above results indicate that $FePO_4$ in SLFP was successfully converted into $LiFePO_4$ after hydrothermal regeneration. The regenerated material was assembled into a battery, and its electrochemical performance is shown in **Figure 16(C)**. The regenerated material exhibits a complete crystal structure, accelerated

interfacial kinetics, and highly reversible lithium-ion intercalation/deintercalation behavior. The effectiveness of the restoration process is evidenced by an initial specific discharge capacity of 138.4 mAh/g and a coulombic efficiency of 99.7%. The capacity retention of the regenerated material was as high as 98.7% after 200 cycles at 1 C.

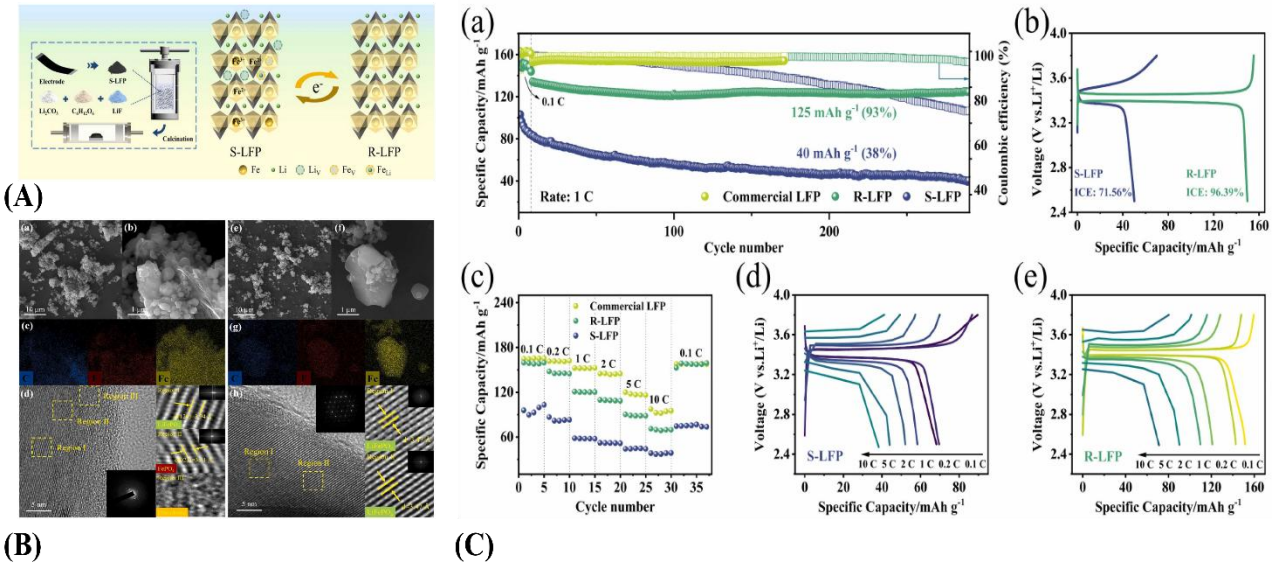

Figure 17 (A) Schematic illustration of targeted hydrothermal repair and regeneration of S-LFP [98]. (B) SEM images of S-LFP (a,b) and R-LFP (e,f). TEM mapping images for C, F and Fe in S-LFP (c) and R-LFP (g). HRTEM images of S-LFP (d) and R-LFP (h) (The images on the right are the HRTEM images of the corresponding regions in the dashed rectangle) [98]. (C) (a) Long-term stability of S-LFP, R-LFP and commercial LFP. Electrodes were cycled at 0.1 C for activation and 1 C for the following cycles, (b) The initial charge and discharge comparison of S-LFP and R-LFP at 0.1 C. (c) Rate capabilities of S-LFP, R-LFP and commercial LFP, The first charge and discharge curves of the LFP at various rates: (d) S-LFP and (e) R-LFP [98].

Song *et al.* [97] utilized lithium from waste graphite obtained from dismantled batteries as the lithium source and citric acid as the reducing agent to regenerate SLFP in a closed-loop hydrothermal method. The lithium extracted from the anode graphite was used as the lithium source, and a mixed solution was prepared with citric acid supplemented with additional $LiOH{\cdot}H_2O$. The LFP was regenerated by heating and reacting with SLFP in a hydrothermal reactor at 180 C for 10 h. Subsequent calcination treatment was done at 700 C. The lattice stripes of the regenerated material were more pronounced, suggesting that the calcination process further improved the crystallinity of the material. The recycled material delivers an outstanding discharge capacity of 139 mAh/g. This excellent performance is owing to the effective two-step hydrothermal-calcination process employed in this work, which successfully reconstructs the cyclically degraded $FePO_4$ phase. The regenerated material features a completely restored crystal structure (Li/Fe molar ratio of 1.02), an optimized carbon coating (ID/IG = 0.8528), a reconstituted microstructure (evidenced by distinct $LiFePO_4$ lattice fringes), and significantly enhanced electrochemical kinetics (polarization voltage of 152.2 mV). These synergistic effects guarantee highly efficient lithium-ion insertion/extraction, leading to the remarkable electrochemical performance. After 100 cycles, the discharge capacity was maintained at 136 mA h/g with a capacity retention rate of 97.8%.

In the process of water/solvent thermal regeneration of SLFP, the residual fluoride in the electrolyte and binder of the used batteries can seriously affect the performance of the regenerated materials. Wu *et al.* [98] obtained fluorinated regenerated materials by introducing additional fluoride during the hydrothermal regeneration process using Li_2CO_3 as the lithium source

and glucose as the reducing agent, and demonstrated that the residual fluoride's had no significant degradation effect on the regenerated materials, as shown in **Figure 17(A)**. SLFP, Li_2CO_3, glucose, and LiF were proportionally added to the hydrothermal reaction device and reacted first at 200 °C for 5 h. The slag was washed to neutrality and dried, and then calcinated under inert gas at 350 and 700 °C for 0.5 h and 2 h, respectively, to obtain F-containing regenerated materials. Scanning electron microscope and TEM images are shown in **Figure 17(B)**, and the regenerated material retained the original particle morphology of $LiFePO_4$ well. In addition, the surface of the regenerated material was smoother and the agglomeration of SLFP particles was reduced. Moreover, the two-stage calcination pretreatment first softens the fluorinated binder in the SLFP at 350 °C, thereby significantly reducing its adhesion to the aluminum foil. This is followed by a high-temperature calcination at 500 °C, which induces rapid and complete decomposition of the PVDF, leading to the removal of the originally fibrous and flocculent binder. Therefore, any residual fluorine-containing substances in the recycled material likely derive from either incompletely removed electrolyte or lithium fluoride incorporation during the hydrothermal process; however, neither source adversely affects the material's microstructure. The electrochemical performance is shown in **Figure 17(C)**, where the initial specific charging capacity of the regenerated material was 134.3 mA h/g. 124.7 mA h/g was retained after 300 cycles, and the battery charging and discharging rate reached 92.85%. Constant-voltage charge/discharge cycles were carried out at a certain current density, and when the current density was suddenly changed from 10 C back to 0.1 C, the regenerated material showed no obvious capacity loss and exhibited excellent multiplicative performance. This indicates that the operation of enhancing the SLFP structure by hydrothermal treatment coupled with short-term annealing repair and introducing F elements in appropriate amounts is feasible, and also implies that a small amount of fluoride ions will not degrade the performance of the regenerated cells.

Electrochemical lithium insertion

During the long-term charging and discharging cycles of lithium iron phosphate batteries, part of the active material transforms into non-capacitive $FePO_4$, leading to a decrease in the capacity of the Li-ion battery. The SLFP battery material has a low energy density and poor stability, but the micro-morphology and crystal structure of the material remain essentially unchanged. This failure mechanism provides a potential method to directly restore SLFP to fresh LFP material, which can be easily used to fabricate new battery cells.Spent lithium iron phosphate (SLFP) exhibits morphological and particle size distribution characteristics similar to those of fresh LFP material. This similarity suggests that the material's physical framework remains intact even after the battery's end of life. The preserved framework allows lithium ions to be re-inserted into the lattice of the spent LFP (which primarily consists of $FePO_4$), thereby regenerating the electrochemically active $LiFePO_4$ phase.

A clever method was proposed by Zhou *et al*, which used electrochemical methods to regenerate the anode lithium/cathode lithium, which used electrochemical methods to regenerate the anode lithium/cathode lithium, as shown in **Figure 18(A)** [99]. An H-type electrolyzer was used as a recycling unit, with zinc plates as the anode, SLFP suspension as the cathode, and Li_2SO_4 as the electrolyte. The relithiation of SLFP was achieved by ensuring the continuous discharge of the electrolyzer through the applied electric field, and the oxidation reaction on the zinc anode provided electrons, which allowed the lithium ions in the electrolyte to be embedded in the SLFP structure.The anode and cathode electrochemical reactions are given by Eqs. (32) - (33).

$$Zn - 2e^- = Zn^{2+} \quad (32)$$

$$Li_{1-x}FePO_4 + xLi^+ + xe^- = LiFePO_4 \quad (33)$$

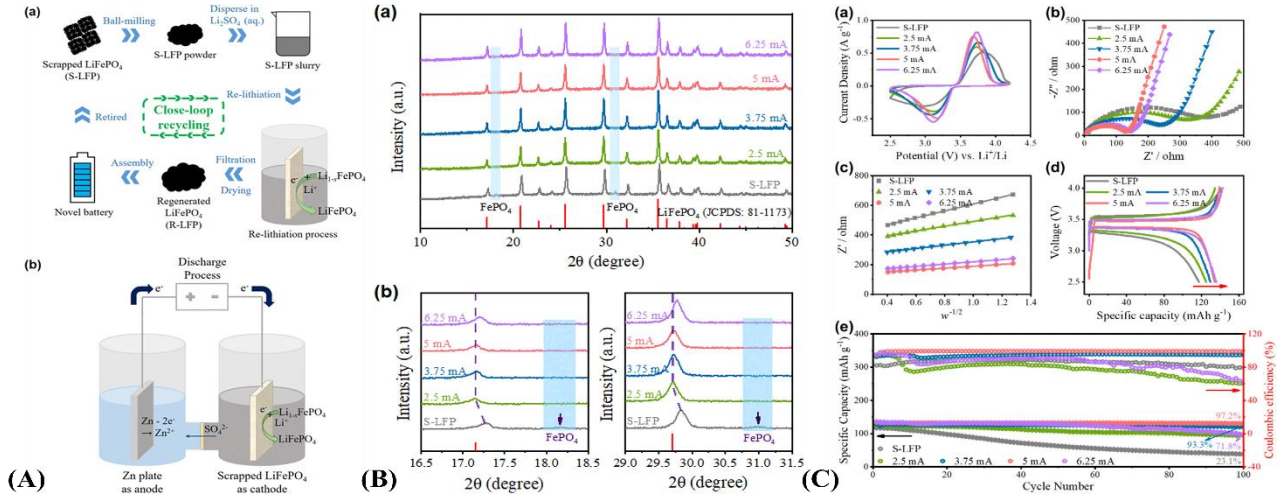

Figure 18 (A) schematic illustration of the direct recycling method. (a) A flow chart of the recycling process and (b) a detailed schematic diagram of the relithiation method [99]. (B) XRD patterns of S-LFP and R-LFP recycled at different currents: (a) the diffraction angle range of 10° to 50° and (b) enlargement of the regions in the range of 16.5° to 18.5° and 29° to 31.5° [99]. (C) 5 Electrochemical performance of S-LFP and R-LFP recycled at different currents. (a) CV curves, (b) EIS profiles, (c) the relationship between Z' and ω−1/2 in the low-frequency region and the corres-ponding fitting lines, (d) the first charge/discharge curves, and (e) the cycling performance at 1C (1C = 170 mAh/g) [99].

However, the residual capacity of different SLFPs varies, leading to differences in the amount of lithium lost in the cathode material. In order to achieve relithiation more accurately and efficiently, the article proposes a factor for the theoretical embedded amount (TIA) of lithium. The purpose of rapid lithium embedding is achieved by controlling 2 parameters, the discharge current size (mA) and the theoretical lithium embedding amount (TIA) during the recycling process. The XRD plots of recycled S-LFP and R-LFP with different discharge current sizes and TIA are shown in **Figure 18(B)**. With the increase of TIA, the peak of $FePO_4$ completely disappears and $LiFePO_4$ is completely generated. This indicates successful Li^+ intercalation, transforming the electrochemically inactive $FePO_4$ into the active $LiFePO_4$. However, when the TIA became excessively high (300%), the peak position shifted to the right. This shift may occur because, at such high TIA levels, excess lithium ions are forcibly intercalated into the crystal lattice. These additional lithium ions may occupy abnormal interstitial sites within the lattice. Such occupation could disrupt crystal order, introducing lattice distortion and internal stress. To release this stress, the crystal may undergo slight lattice contraction, leading to a decrease in the interplanar spacing d. This is reflected in the XRD pattern as a rightward shift of the diffraction peaks. The structure of R-LFP is affected, which suggests that excessive lithium embedding is not conducive to lithium replenishment, but the exact reason is still to be investigated. $FePO_4$ in cyclic SLFP is transformed to $LiFePO_4$ at different discharge current sizes, and R-LFP conforms to the olivine structure of LFP, which is consistent with previous experimental findings. In addition, the relithiation time can be reduced at higher discharge currents to lower the cost, and it also facilitates the embedding of lithium ions. The electrochemical test performance of S-LFP and R-LFP recirculated at different discharge current magnitudes with TIA is shown in **Figure 18(C)**. The optimal reaction conditions are: Discharge current of 5 mA and TIA of 150%. The best-performing R-LFP material can be obtained with a discharge capacity of up to 134.0 mA h/g at 1 C and a capacity retention of 85.5% after 300 cycles. The efficient regeneration of SLFP using low-cost and green aqueous solution as electrolyte also provides a new idea for the recovery of other cathode materials from SLIB. Different methods for direct regeneration of $LiFePO_4$ materials are shown in **Table 6**.

Table 6 Different methods of direct regeneration of $LiFePO_4$ materials.

Direct recycling	Materials	Conditions	Performance	References
Solid-phase sintering	Li_2CO_3, CNTs, $C_6H_{12}O_6$	350 ℃, 2 h then 650 ℃, 12 h	155.47 mA h/g at 0.05 C.	[94]
	CH_3OH, $C_6H_8O_7$	650 ℃, 2 h	141.5 mA h/g at 1 C.	[95]
Hydro/solvent-thermal regeneration	$LiOH·H_2O$, dl-$C_4H_6O_5$	1.2 mol/L Li^+, 100 ℃, 6 h	158.5, 155.3, 149.5, 142.4, 131.8, 108.6, 70.8 mA h/g at 0.1, 0.2, 0.5 ,1, 2, 5 and 10 C.	[96]
	$LiOH·H_2O$, $C_6H_8O_7$	180 ℃ for 10 h, then 350 ℃ for 3 h, finally, 700 ℃	139 mA h/g at 0.5 C.	[97]
	Li_2CO_3, $C_6H_{12}O_6$	200 ℃ for 5 h, 350 ℃, 30 min, 700 ℃, 2 h	159.56 mA h/g at 0.1 C.	[98]
Electrochemical lithiation	Zn plate, Li_2SO_4	A current of 5 mA and 150%-TIA	134.0 mA h/g at 1 C.	[99]

Challenges, future directions and conclusions

This paper presents a comprehensive review of mainstream process technologies for recycling spent lithium iron phosphate (SLFP) batteries. Hydrometallurgical recovery and direct regeneration are identified as the most promising routes for future industrial applications. A notable paradigm shift is underway, moving from the traditional "leaching-impurity removal-separation" approach, which relies on complex separation steps, toward more efficient strategies centered on "selective leaching" and "direct regeneration." The optimal pathway for SLFP resource utilization lies in regenerating high-performance LFP cathode materials via elemental compensation, structural repair, or the direct use of intermediate lithium-iron-phosphate compounds. Nevertheless, current research has not yet fully satisfied the demands of industrialization, and individual recycling technologies still face challenges in concurrently achieving economic viability and the high-value utilization of all recovered products. To facilitate the integrated recycling of SLFP and support the sustainable development of the lithium-ion battery industry, we propose the following outlook:

(1) Intelligent separation and synergistic recovery for complex systems

The increasing diversification of battery material systems (e.g., blends of lithium iron phosphate with ternary materials or lithium manganese oxide) necessitates a shift in recycling technologies from single-component to mixed-waste processing. Future research should prioritize the development of universal or intelligently responsive recycling systems capable of adapting to various cathode materials. The objective is to create systems that, based on the distinct properties of different metal ions (such as coordination preference and redox potential), can achieve single-step selective leaching of valuable metals (e.g., Li, Ni, Co, Mn) alongside the in-situ separation of impurity elements (e.g., Fe, Al, Cu).

(2) Deep development and integration of green, low-energy leaching technologies

Conventional strong acid leaching processes are plagued by significant environmental and economic drawbacks. Future research should prioritize the innovation of the leaching technologies per se, shifting the focus toward greener alternatives that feature low energy consumption, minimal pollution, and reduced corrosivity. A key direction involves developing coupled systems that integrate novel green solvents (e.g., deep eutectic solvents, DES) with clean energy inputs (e.g., photocatalysis, electrochemistry, ultrasound) and clean oxidants (e.g., O_3). Leveraging external field enhancement and synergistic reaction mechanisms, this strategy aims to achieve substantial improvements in the selectivity, efficiency, and kinetics of lithium leaching under mild conditions.

(3) Integration of closed-loop recycling and short-process reprocessing technologies

The ultimate objective of recycling should evolve from mere metal recovery to the direct regeneration of high-value cathode materials, thereby establishing a

closed-loop cycle from spent batteries to new products. Future technological development must, therefore, integrate leaching, purification, and material re-synthesis into a cohesive system, promoting short-process, integrated technologies. The aim is to minimize intermediate steps by directly converting the purified leachate or immobilized intermediates (e.g., $FePO_4$) into electrochemically active precursor or final cathode materials.

In summary, the field of spent lithium iron phosphate (LFP) battery recycling is undergoing a significant transformation, moving decisively toward precision recycling guided by the principles of green chemistry. This evolution is characterized by the pursuit of greener leaching agents, more selective processes, and closed-loop pathways. The paradigm is shifting from simple "metal extraction" to direct "material regeneration," whereby leaching outputs (e.g., purified lithium solution and $FePO_4$ residue) are converted into high-performance cathode materials via short-process workflows, thereby establishing a "waste-to-product" circular economy model. The successful development of systems like deep eutectic solvents (DES) and glycine leaching not only provides more economical and environmentally benign technical routes for LFP recycling but, more importantly, showcases a viable approach to addressing practical environmental problems through the innovative application of fundamental chemistry. Future breakthroughs will likely depend on three key areas: the development of universal, intelligent recycling systems for mixed battery waste; a deeper mechanistic understanding of green leaching technologies; and the advancement of fully integrated recycling and direct regeneration processes

Acknowledgements

This work was supported by Jiangsu University and Zhejiang New Era Zhongneng Co., Ltd. The overall research objectives were proposed by Aichun Dou, Luping Liu, and Zhixiong Yan. Qingshan Du provided literature analysis and verification, Yunjian Liu offered financial support, and Yuqian Fan and Jianze Bai conducted data organization. The initial draft manuscript was authored by Qingshan Du. All authors responded to reviewers' comments and revised the final version.

CRediT author statement

Aichun Dou: Data curation; Investigation; Writing-original draft. **Qingshan Du:** Investigation; Formal analysis; Visualization; Writing-original draft. **Zhixiong Yan:** Resources. **Yunjian Liu:** Funding acquisition. **Luping Liu:** Writing – Review & Editing. **Yuqian Fan:** Visualization. Zejian Bai: Supervision.

References

[1] MM Alam, H Huang, Z Yang, L Zou, Z Chi and W Zhang. Innovative green intense tetra-eutectic solvent (ITES) for recovery via occlusion co-precipitation at room temperature. *Sustainable Materials and Technologies* 2024; **40**, 14643.

[2] A Paolella, C Faure, G Bertoni, S Marras, A Guerfi, A Darwiche, P Hovington, B Commarieu, Z Wang, M Prato, M Colombo, S Monaco, W Zhu, Z Feng, A Vijh, C George, GP Demopoulos, M Armand and K Zaghib. Light-assisted delithiation of lithium iron phosphate nanocrystals towards photo-rechargeable lithium-ion batteries. *Nature Communications* 2017; **8**, 14643.

[3] T Naseri and SM Mousavi. Treatment of spent lithium iron phosphate (LFP) batteries. *Current Opinion in Green and Sustainable Chemistry* 2024; **47**, 100906.

[4] H Jiangyi and W Fan. Design and testing of a small orchard tractor driven by a power battery. *Engenharia Agricola* 2023; **43(2)**, e20220195.

[5] Q Wu, Y Zhong, R Chen, G Ling, X Wang, Y Shen and C Hao. Cu-Ag-C@Ni3S4 with core shell structure and rose derived carbon electrode materials: An environmentally friendly supercapacitor with high energy and power density. *Industrial Crops and Products* 2024; **222**, 119676.

[6] X Wang, Y Pan, X Wang, Y Guo, C Ni, J Wu and C Hao. High performance hybrid supercapacitors assembled with multi-cavity nickel cobalt sulfide hollow microspheres as cathode and porous typha-derived carbon as anode. *Industrial Crops and Products* 2022; **189**, 115863.

[7] RC Wang, YC Lin and SH Wu. A novel recovery process of metal values from the cathode active materials of the lithium-ion secondary batteries. *Hydrometallurgy* 2009; **99(3-4)**, 194-201.

[8] K Cui, MC Zhao, Y Li, A Atrens and F Zhang. Recycling of spent lithium iron phosphate batteries: Research progress based on environmental protection and sustainable development technology. *Separation and Purification Technology* 2025; **354**, 128982.

[9] AS Andersson, JO Thomas, B Kalska and L Häggström. Thermal stability of $LiFePO_4$-based cathodes. *Electrochemical and Solid-State Letters* 2000; **3(2)**, 66-68.

[10] Y Wang, N An, L Wen, L Wang, X Jiang, F Hou, Y Yin and J Liang. Recent progress on the recycling technology of Li-ion batteries. *Journal of Energy Chemistry* 2021; **55**, 391-419.

[11] T Or, SWD Gourley, K Kaliyappan, A Yu and Z Chen. Recycling of mixed cathode lithium-ion batteries for electric vehicles: Current status and future outlook. *Carbon Energy* 2020; **2(1)**, 6-43.

[12] MG Moustafa and MMS Sanad. Green fabrication of $ZnAl_2O_4$-coated $LiFePO_4$ nanoparticles for enhanced electrochemical performance in Li-ion batteries. *Journal of Alloys and Compounds* 2022; **903**, 163910.

[13] W Shen, W Han, TJ Wallington and SL Winkler. China electricity generation greenhouse gas emission intensity in 2030: implications for electric vehicles. *Environmental Science & Technology* 2019; **53(10)**, 6063-6072.

[14] SW Kim, SG Park and EJ Lee. Assessment of the explosion risk during lithium-ion battery fires. *Journal of Loss Prevention in the Process Industries* 2022; **80**, 104851.

[15] X Chen, D Kang, J Li, T Zhou and H Ma. Gradient and facile extraction of valuable metals from spent lithium ion batteries for new cathode materials re-fabrication. *Journal of Hazardous Materials* 2020; **389**, 121887.

[16] K He, ZY Zhang and FS Zhang. Selectively peeling of spent $LiFePO_4$ cathode by destruction of crystal structure and binder matrix for efficient recycling of spent battery materials. *Journal of Hazardous Materials* 2020; **386**, 121633.

[17] S Natarajan and V Aravindan. Burgeoning prospects of spent lithium-ion batteries in multifarious applications. *Advanced Energy Materials* 2018; **8(33)**, 1802303.

[18] CP Makwarimba, M Tang, Y Peng, S Lu, L Zheng, Z Zhao and A Zhen. Assessment of recycling methods and processes for lithium-ion batteries. *Iscience* 2022; **25(5)**, 104321.

[19] L Yang, G Xi and Y Xi. Recovery of Co, Mn, Ni, and Li from spent lithium ion batteries for the preparation of $LiNi_xCo_yMn_zO_2$ cathode materials. *Ceramics International* 2015; **41(9)**, 11498-11503.

[20] J Ordoñez, EJ Gago and A Girard. Processes and technologies for the recycling and recovery of spent lithium-ion batteries. *Renewable & Sustainable Energy Reviews* 2016; **60**, 195-205.

[21] M Fan, X Chang, YJ Guo, WP Chen, YX Yin, X Yang, Q Meng, LJ Wan and YG Guo. Increased residual lithium compounds guided design for green recycling of spent lithium-ion cathodes. *Energy & Environmental Science* 2021; **14(3)**, 1461-1468.

[22] Z Huang, F Liu, B Makuza, D Yu, X Guo and Q Tian. Metal reclamation from spent lithium-ion battery cathode materials: Directional conversion of metals based on hydrogen reduction. *ACS Sustainable Chemistry & Engineering* 2022; **10(2)**, 756-765.

[23] B Makuza, Q Tian, X Guo, K Chattopadhyay and D Yu. Pyrometallurgical options for recycling spent lithium-ion batteries: A comprehensive review. *Journal of Power Sources* 2021; **491**, 229622.

[24] G Zhang, Z Liu, X Yuan, Y He, N Wei, H Wang and B Zhang. Recycling of valuable metals from spent cathode material by organic pyrolysis combined with in-situ thermal reduction. *Journal of Hazardous Materials* 2022; **430**, 128374.

[25] H Sahivirta, BP Wilson, M Lundström and R Serna-Guerrero. A study on recovery strategies of graphite from mixed lithium-ion battery chemistries using froth flotation. *Waste Management* 2024; **180**, 96-105.

[26] S Jiang, X Li, Q Gao, X Lyu, SN Akanyange, T Jiao and X Zhu. Review on full-component green recycling of spent lithium iron phosphate cathode materials: From the perspective of economy and efficiency. *Separation and Purification Technology* 2023; **324**, 124630.

[27] H Wang, Z Li, Q Meng, J Duan, M Xu, Y Lin and Y Zhang. Ammonia leaching of valuable metals from spent lithium ion batteries in NH_3-$(NH_4)_2SO_4$-Na_2SO_3 system. *Hydrometallurgy* 2022; **208**, 105809.

[28] D Song, T Wang, Z Liu, S Zhao, J Quan, G Li, H Zhu, J Huang and W He. Characteristic comparison of leaching valuable metals from spent power Li-ion batteries for vehicles using the inorganic and organic acid system. *Journal of Environmental Chemical Engineering* 2022; **10(1)**, 107102.

[29] JJ Roy, S Rarotra, V Krikstolaityte, KW Zhuoran, YDI Cindy, XY Tan, M Carboni, D Meyer, Q Yan and M Srinivasan. Green recycling methods to treat lithium-ion batteries e-waste: A circular approach to sustainability. *Advanced Materials* 2022; **34(25)**, 2103346.

[30] J Zhao, B Zhang, H Xie, J Qu, X Qu, P Xing and H Yin. Hydrometallurgical recovery of spent cobalt-based lithium-ion battery cathodes using ethanol as the reducing agent. *Environmental Research* 2020; **181**, 108803.

[31] Z Li, L He, Y Zhu and C Yang. A green and cost-effective method for production of LiOH from spent $LiFePO_4$. *ACS Sustainable Chemistry & Engineering* 2020; **8(42)**, 15915-15926.

[32] J Yu, X Wang, M Zhou and Q Wang. A redox targeting-based material recycling strategy for spent lithium ion batteries. *Energy & Environmental Science* 2019; **12(9)**, 2672-2677.

[33] S Jiang, C Nie, X Li, S Shi, Q Gao, Y Wang, X Zhu and Z Wang. Review on comprehensive recycling of spent lithium-ion batteries: A full component utilization process for green and sustainable production. *Separation and Purification Technology* 2023; **315**, 123684.

[34] E Fan, J Yang, Y Huang, J Lin, F Arshad, F Wu, L Li and R Chen. Leaching mechanisms of recycling valuable metals from spent lithium-ion batteries by a malonic acid-based leaching system. *ACS Applied Energy Materials* 2020; **3(9)**, 8532-8542.

[35] N Bahaloo-Horeh, SM Mousavi and M Baniasadi . Use of adapted metal tolerant *Aspergillus niger* to enhance bioleaching efficiency of valuable metals from spent lithium-ion mobile phone batteries. *Journal of Cleaner Production* 2018; **197**, 1546-1557.

[36] Z Ou, J Li and Z Wang. Application of mechanochemistry to metal recovery from second-hand resources: A technical overview. *Environmental Science-Processes & Impacts* 2015; **17(9)**, 1522-1530.

[37] J Neumann, M Petranikova, M Meeus, JD Gamarra, R Younesi, M Winter and S Nowak. Recycling of lithium-ion batteries-current state of the art, circular economy, and next generation recycling. *Advanced Energy Materials* 2022; **12(17)**, 2102917.

[38] N Tolganbek, N Zhalgas, Y Kadyrov, N Umirov, Z Bakenov and A Mentbayeva. Facile deposition of the $LiFePO_4$ cathode by the electrophoresis method. *ACS Omega* 2023; **8(8)**, 8045-8051.

[39] D Bian, Y Sun, S Li, Y Tian, Z Yang, X Fan and W Zhang. A novel process to recycle spent $LiFePO_4$ for synthesizing $LiFePO_4$/C hierarchical microflowers. *Electrochimica Acta* 2016; **190**, 134-140.

[40] W Song, J Liu, L You, S Wang, Q Zhou, Y Gao, R Yin, W Xu and Z Guo. Re-synthesis of nano-structured $LiFePO_4$/graphene composite derived from spent lithium-ion battery for booming electric vehicle application. *Journal of Power Sources* 2019; **419**, 192-202.

[41] Q Sun, X Li, H Zhang, D Song, X Shi, J Song, C Li and L Zhang. Resynthesizing $LiFePO_4$/C materials from the recycled cathode via a green full-solid route. *Journal of Alloys and Compounds* 2020; **818**, 153292.

[42] Q Wang, B Mao, SI Stoliarov and J Sun. A review of lithium ion battery failure mechanisms and fire prevention strategies. *Progress in Energy and Combustion Science* 2019; **73**, 95-131.

[43] LP Yao, Q Zeng, T Qi and J Li. An environmentally friendly discharge technology to pretreat spent lithium-ion batteries. *Journal of Cleaner Production* 2020; **245**, 118820.

[44] Y Gou, J Zhang, X Liu, Z Zhou, M Zhang, L Song and Y Jin. A Highly efficient additive for direct reactivation of waste $LiFePO_4$ with practical electrochemical performance. *Energy Fuel* 2024; **38(7)**, 6518-6527.

[45] B Chen, M Liu, S Cao, H Hu, G Chen, X Guo and X Wang. Direct regeneration and performance of spent $LiFePO_4$ via a green efficient hydrothermal technique. *Journal of Alloys and Compounds* 2022; **924**, 166487.

[46] Y Yang, J Zhang, H Zhang, Y Wang, Y Chen and C Wang. Simultaneous anodic de-lithiation/cathodic lithium-embedded regeneration method for recycling of spent $LiFePO_4$ battery. *Energy Storage Materials* 2024; **65**, 103081.

[47] KC Chiu, CH Lin, SF Yeh, YH Lin and KC Chen. An electrochemical modeling of lithium-ion battery nail penetration. *Journal of Power Sources* 2014; **251**, 254-263.

[48] D Yu, Z Huang, B Makuza, X Guo and Q Tian. Pretreatment options for the recycling of spent lithium-ion batteries: A comprehensive review. *Minerals Engineering* 2021; **173**, 107218.

[49] D Saju, J Ebenezer, N Chandran and N Chandrasekaran. Recycling of lithium iron phosphate cathode materials from spent lithium-ion batteries: A mini-review. *Industrial & Engineering Chemistry Research* 2023; **62(30)**, 11768-11783.

[50] J Xu, HR Thomas, RW Francis, KR Lum, J Wang and B Liang. A review of processes and technologies for the recycling of lithium-ion secondary batteries. *Journal of Power Sources* 2008; **177(2)**, 512-527.

[51] T Zhao, R Marthi, H Mahandra, S Chae, M Traversy, F Sadri, Y Choi and A Ghahreman. Direct selective leaching of lithium from industrial-grade black mass of waste lithium-ion batteries containing $LiFePO_4$ cathodes. *Waste Management* 2023; **171**, 134-142.

[52] T Gao, T Dai, N Fan, Z Han and X Gao. Comprehensive review and comparison on pretreatment of spent lithium-ion battery. *Journal of Environmental Management* 2024; **363**, 121314.

[53] J Nan, D Han and X Zuo. Recovery of metal values from spent lithium-ion batteries with chemical deposition and solvent extraction. *Journal of Power Sources* 2005; **152(1)**, 278-284.

[54] R Zhan, Z Oldenburg and L Pan. Recovery of active cathode materials from lithium-ion batteries using froth flotation. *Sustainable Materials and Technologies* 2018; **17**, e00062.

[55] MP Dos Santos, IAA Garde, CMB Ronchini, L Cardozo Filho, GBM De Souza, MLF Abbade, NN Regone, V Jegatheesan and JA de Oliveira. A technology for recycling lithium-ion batteries promoting the circular economy: The RecycLib. *Resources Conservation and Recycling* 2021; **175**, 105863.

[56] J Xiao, J Guo, L Zhan and Z Xu. A cleaner approach to the discharge process of spent lithium ion batteries in different solutions. *Journal of Cleaner Production* 2020; **255**, 120064.

[57] N Garg, S Pekkinen, EM González, R Serna-Guerrero, P Peljo and A Santasalo-Aarnio. Enhanced electrochemical discharge of Li-ion batteries for safe recycling. *Sustainable Energy & Fuels* 2024; **8(12)**, 2777-2788.

[58] K Liivand, M Kazemi, P Walke, V Mikli, M Uibu, DD Macdonald and I Kruusenberg. Spent Li-ion battery graphite turned into valuable and active catalyst for electrochemical oxygen reduction. *Chemsuschem* 2021; **14(4),** 1103-1111.

[59] S Kumawat, D Singh and A Saini. Recycling of spent lithium-iron phosphate batteries: toward closing the loop. *Materials and Manufacturing Processes* 2023; **38(2)**, 135-150.

[60] Y Jie, S Yang, Y Li, F Hu, D Zhao, D Chang, Y Lai and Y Chen. Waste organic compounds thermal treatment and valuable cathode materials recovery from spent $LiFePO_4$ batteries by vacuum pyrolysis. *ACS Sustainable Chemistry & Engineering* 2020; **8(51)**: 19084-19095.

[61] TRB Grandjean, J Groenewald and J Marco. The experimental evaluation of lithium-ion batteries after flash cryogenic freezing. *Journal of Energy Storage* 2019; **21**, 202-215.

[62] LP He, SY Sun, XF Song and JG Yu. Recovery of cathode materials and Al from spent lithium-ion batteries by cleaning. *Waste Management* 2015; **46**, 523-528.

[63] D Fu, W Zhou, J Liu, S Zeng, L Wang, W Liu, X Yu and X Liu. A facile route for the efficient leaching, recovery, and regeneration of lithium and iron from waste lithium iron phosphate cathode materials. *Separation and Purification Technology* 2024; **342**, 127069.

[64] B Zhang, X Qu, X Chen, D Liu, Z Zhao, H Xie, D Wang and H Yin. A sodium salt-assisted roasting approach followed by leaching for recovering spent $LiFePO_4$ batteries. *Journal of Hazardous Materials* 2022; **424**, 127586.

[65] X Qu, J Ma, B Zhang, J Zhao, B Qiu, X Chen, F Zhou, X Li, S Gao, D Wang and H Yin. Fast ammonium sulfate salt assisted roasting for selectively recycling degraded $LiFePO_4$ cathode. *Journal of Cleaner Production* 2024; **435**, 140428.

[66] L Zhang, T Teng, L Xiao, L Shen, J Ran, J Zheng, Y Zhu and H Chen. Recovery of $LiFePO_4$ from used lithium-ion batteries by sodium-bisulphate-assisted roasting. *Journal of Cleaner Production* 2022; **379**, 134748.

[67] X Li, F Zhou, S Gao, J Zhao, D Wang and H Yin. NaOH-assisted low-temperature roasting to recover spent $LiFePO_4$ batteries. *Waste Management* 2022; **153**, 347-354.

[68] H Hu, X Meng, Y Li, Y Yang, Y Xu, J Hu and Y Yao. Potassium pyrosulfate-assisted roasting and water leaching for selectively Li and Fe recycling from spent $LiFePO_4$ batteries. *Acs Sustainable Chemistry & Engineering* 2024; **12(45)**, 16553-16563.

[69] H Li, H Ye, M Sun and W Chen. Process for recycle of spent lithium iron phosphate battery via a selective leaching-precipitation method. *Journal of Central South University* 2020; **27(11)**, 3239-3248.

[70] DF Wang, M Chen, JJ Zhao, FY Zhou, HY Wang, X Qu, YQ Cai, ZY Zheng, DH Wang and HY Yin. Revealing role of oxidation in recycling spent lithium iron phosphate through acid leaching. *Rare Metals* 2024; **44(3)**, 2059-2070.

[71] X Dai, T Qi, X Li, Z Peng, G Liu, Q Zhou, Y Wang and L Shen. Selective leaching of lithium from mixed spent lithium iron phosphate powder. *Journal of Environmental Chemical Engineering* 2024; **12(5)**, 114091.

[72] W Liu, K Li, W Wang, Y Hu, Z Ren and Z Zhou. Selective leaching of lithium ions from $LiFePO_4$ powders using hydrochloric acid and sodium hypochlorite system. *Canadian Journal of Chemical Engineering* 2023; **101(4)**, 1831-1841.

[73] Y Yang, X Meng, H Cao, X Lin, C Liu, Y Sun, Y Zhang and Z Sun. Selective recovery of lithium from spent lithium iron phosphate batteries: A sustainable process. *Green Chemistry* 2018; **20(13)**, 3121-3133.

[74] Y Dai, Z Xu, D Hua, H Gu and N Wang. Theoretical-molar Fe^{3+} recovering lithium from spent $LiFePO_4$ batteries: An acid-free, efficient, and selective process. *Journal of Hazardous Materials* 2020; **396**, 122707

[75] J Zhang, J Hu, Y Liu, Q Jing, C Yang, Y Chen and C Wang. Sustainable and facile method for the selective recovery of lithium from cathode scrap of spent $LiFePO_4$ batteries. *ACS Sustainable Chemistry & Engineering* 2019; **7(6)**, 5626-5631.

[76] W Gao, J Song, H Cao, X Lin, X Zhang, X Zheng, Y Zhang and Z Sun. Selective recovery of valuable metals from spent lithium-ion batteries - Process development and kinetics evaluation. *Journal of Cleaner Production* 2018; **178**, 833-845.

[77] W Urbańska. Recovery of Co, Li, and Ni from spent li-ion batteries by the inorganic and/or organic reducer assisted leaching method. *Minerals* 2020; **10(6)**, 555

[78] G Ji, J Wang, Z Liang, K Jia, J Ma, Z Zhuang, G Zhou and HM Cheng. Direct regeneration of degraded lithium-ion battery cathodes with a multifunctional organic lithium salt. *Nature Communications* 2023; **14(1)**, 584

[79] G Ji, X Ou, R Zhao, J Zhang, J Zou, P Li, D Peng, L Ye, B Zhang and D He. Efficient utilization of scrapped $LiFePO_4$ battery for novel synthesis of $Fe_2P_2O_7$/C as candidate anode materials. *Resources Conservation and Recycling* 2021; **174**, 105802.

[80] Y Yang, X Meng, H Cao, X Lin, C Liu, Y Sun, Y Zhangab and Z Sun. Selective recovery of lithium from spent lithium iron phosphate batteries: a sustainable process. *Green Chemistry* 2018; **20(13)**, 3121-3133.

[81] J Zhou, H Yu, Y Mei, L Xu, L Liu, J Hu, H Hou and J Yang. Green recovery of metals from spent lithium iron phosphate cathode by organic acid leaching. *Modern Chemical Industry* 2024; **44(11)**, 202-207.

[82] E Fan, L Li, X Zhang, Y Bian, Q Xue, J Wu, F Wu and R Chen. Selective recovery of Li and Fe from spent lithium-ion batteries by an environmentally friendly mechanochemical approach. *Acs*

Sustainable Chemistry & Engineering 2018; **6(8)**, 11029-11035.

[83] YH Wang, JJ Wu, GC Hu and W Ma. Recovery of Li and Fe from spent lithium iron phosphate using organic acid leaching system. *Transactions of Nonferrous Metals Society of China* 2024; **34(1)**, 336-346.

[84] AP Abbott, G Capper, DL Davies, RK Rasheed and V Tambyrajah. Novel solvent properties of choline chloride/urea mixtures. *Chemical Communications* 2003; **1**, 70-71.

[85] Y Liao, S Gong, G Wang, T Wu, X Meng, Q Huang, Y Su, F Wu and RM Kelly. A novel ternary deep eutectic solvent for efficient recovery of critical metals from spent lithium-ion batteries under mild conditions. *Journal of Environmental Chemical Engineering* 2022; **10(6)**, 108627.

[86] S Tang, Z Yang, M Zhang and M Guo. A simple green method for *in-situ* selective extraction of Li from spent $LiFePO_4$ batteries by synergistic effect of deep-eutectic solvent and ozone. *Ervironmental Research* 2023; **239**, 117393

[87] T Or, SWD Gourley, K Kaliyappan, A Yu and Z Chen. Recycling of mixed cathode lithium-ion batteries for electric vehi-cles: Current status and future outlook. *Carbon Energy* 2020; **2(1)**, 6.

[88] JM Peng, ZQ Chen, Y Li, SJ Hu, QC Pan, FH Zheng, HQ Wang and QY Li. Conducting network interface modulated rate performance in $LiFePO_4$/C cathode materials. *Rare Metals* 2022; **41(3)**, 951

[89] JF Whitacre, K Zaghib, WC West and BV Ratnakumar. Dual active material composite cathode structures for Li-ion batteries. *Journal of Power Sources* 2008; **177(2)**, 528.

[90] KG Gallagher, SH Kang, SU Park and SY Han. $xLi_2MnO_{3(1-x)}LiMO_2$ blended with $LiFePO_4$ to achieve high energy density and pulse power capability. *Journal of Power Sources* 2011; **196(22)**, 9702.

[91] J Zheng, X Li, Z Wang, S Niu, D Liu, L Wu, L Li, J Li and H Guo. Novel synthesis of $LiFePO_4$-$Li_3V_2(PO_4)_3$ com- posite cathode material by aqueous precipitation and lithiation. *Journal of Power Sources* 2010; **195(9)**, 2935.

[92] S Kim. The reduction of formaldehyde and VOCs emission from wood-based flooring by green adhesive using cashew nut shell liquid (CNSL). *Journal of Hazardous Materials* 2010; **182(1-3)**, 919.

[93] D Ai-Chun, F Yu-Qian, K Xiao, C Yao-Dong, Q Ji-Kai, L Yun-Jian, SU Ming-Ru, Z Yu and Z Xiao-Chao. Selective leaching of valuable metal from spent lithium-ion batteries in the alkaline glycinate system. *Journal of Central South University* 2025; **32(05)**, 1710-1723.

[94] L Song, C Qi, S Wang, X Zhu, T Zhang, Y Jin and M Zhang. Direct regeneration of waste $LiFePO_4$ cathode materials with a solid-phase method promoted by activated CNTs. *Waste Management* 2023; **157**, 141-148.

[95] Y Han, Y Fang, M Yan, H Qiu, Y Han, Y Chen, L Lin, J Qian, T Mei and X Wang. Direct regeneration of fluorine-doped carbon-coated $LiFePO_4$ cathode materials from spent lithium-ion batteries. *Green Chemistry* 2024; **26(18)**, 9791-9801.

[96] J Yang, K Zhou, R Gong, Q Meng, Y Zhang and P Dong. Direct regeneration of spent $LiFePO_4$ materials via a green and economical one-step hydrothermal process. *Journal of Environmental Management* 2023; **348**, 119384.

[97] J Song, M Xiao, T Chen, F Wan and X Guo. Regeneration of degraded lithium iron phosphate by utilizing residual lithium from spent graphite anode. *Materials Letters* 2024; **363**, 136333.

[98] Y Wu, S Mao, S Xu, Q Yuan, T Xiao, Y Li, Z Wang, Q Sui, B Yuan, H Wen an J Liu. Enhanced rate performance of fluoride-containing spent $LiFePO_4$ through direct hydrothermal regeneration. *Journal of Environmental Chemical Engineering* 2025; **13(1)**, 115057.

[99] S Zhou, J Du, X Xiong, L Liu, J Wang, L Fu, J Ye, Y Chen and Y Wu. Direct recovery of scrapped $LiFePO_4$ by a green and low-cost electrochemical re-lithiation method. *Green Chemistry* 2022; **24(16)**, 6278-6286.